Materials and Structures (2022)55:149
https://doi.org/10.1617/s11527-022-01973-1

Paper of RILEM TC 282-CCL: mineralogical characterization methods for clay resources intended for use as supplementary cementitious material

Ruben Snellings · Roger Almenares Reyes · Theodore Hanein · Edgardo F. Irassar · Fragkoulis Kanavaris · Matthias Maier · Alastair T. Marsh · Luca Valentini · Franco Zunino · Adrian Alujas Diaz

Received: 3 January 2022 / Accepted: 25 April 2022

Abstract To respond to the rapid introduction and development of calcined clays as supplementary cementitious material (SCM), the toolbox of characterization methods for cementitious materials requires extension to raw clay characterization. Borrowing concepts and methods developed in the field of clay mineralogy, this paper outlines the merits and limits of widely accessible characterization techniques for raw clays intended for use as SCM, when calcined. The paper focuses mainly on the identification and quantification of the raw clay mineral components, as these characteristics have important implications for further material processing and performance. General notes are provided on clay sampling and pre-treatment as well as bulk chemical analysis. The main techniques considered are X-ray diffraction, thermal analysis and infrared spectroscopy. Their application on raw clays is introduced, highlighting clay-specific aspects of

This paper has been prepared by working group 1 within RILEM TC 282-CCL. The paper has been reviewed and approved by all members of the TC.
TC Membership:
Chair Prof. Fernando Martirena-Hernandez
Deputy Chair Prof. Manu Santhanam
Members: Sumaiya Afroz, Laith Al-Jaberi, Adrian Alujas-Diaz, Francois Avet, Tushar Bansal, Hoda Beltagui, Mohsen Ben Haha, Susan Bernal Lopez, Shashank Bishnoi, Pascal Boustingorry, Mariana Canut, Arnaud Castel, Vinh Dao, Frank Dehn, Yuvaraj Dhandapani, Pascal Dion, Jan Elsen, Gilles Escadeillas, J Ivan Escalante-Garcia, Hassan Ez-Zaki, Sergio Ferreiro Garzón, Daniel Geddes, Guoqing Geng, Ravindra Gettu, Theodore Hanein, Edgardo Irassar, Roman Jaskulski, Shiju Joseph, Maria C. Garcia Juenger, Sri Kalyana Rama Jyosyula, Fragkoulis Kanavaris, Taehwan Kim, Wolfgang Kunther, David Law, Alisa Machner, Matthias Maier, Alastair Marsh, Fabrizio Moro, Joseph Mwiti Marangu, Angela Nunes, Katelyn O Quinn, Anuj Parashar, Gabriel Pham, Victor Poussardin, John Provis, Elsa Qoku, Kyle Riding, Roger Almenares Reyes, Karyne Ferreira dos Santos, Karen Scrivener, Jorgen Skibsted, Ruben Snellings, Tongbo Sui, Arezki Tagnit-Hamou, Karl-Christian Thienel, Luca Valentini, Oscar Oswaldo Vazquez, Luis Velasquez, Manuel Vieira, Silvia Vieira, Talakokula Visalakshi, Claire White, William Wilson, Kequan Yu, Zengfeng Zhao, Wenzhong Zhu, and Franco Zunino.

R. Snellings (✉)
Sustainable Materials, VITO, Mol, Belgium
e-mail: ruben.snellings@vito.be

R. Almenares Reyes
Instituto Superior Minero Metalúrgico de Moa, Moa, Cuba

T. Hanein
Department of Materials Science and Engineering, University of Sheffield, Sheffield, UK

E. F. Irassar
Departamento de Ingeneria Civil, National University of the Center of the Buenos Aires Province, Olavarria, Argentina

F. Kanavaris
ARUP, London, UK

Published online: 15 June 2022

sample preparation, data acquisition, and processing. Guidelines and interpretation tables are provided to aid in the analysis of the acquired data, while limitations and potential interferences are identified. Options for remote prospection by infrared spectroscopy are included as well. To illustrate the type of information to be gained and the complementarity of the techniques, two representative raw clays are fully characterised. This paper aims to highlight that mineralogical characterization is a feasible and often necessary step in the study and assessment of raw clays that can deliver a wealth of informative data if carried out appropriately.

Keywords Clay · Characterisation · Mineralogy · Cement · Supplementary cementitious materials

1 Introduction

Relevant and reliable data are a cornerstone of scientific progress and industrial or governmental decision-making. Acquisition, processing, and interpretation of raw data are therefore key aspects of scientific practice and most disciplines have developed tailored sets of test methods and techniques adapted to the field of study. This set of tests is subject to continuous adaptation in response to technical developments and extensions or shifts of scope of the field.

M. Maier
University of the Bundeswehr Munich, Neubiberg, Germany

A. T. Marsh
School of Civil Engineering, University of Leeds, Leeds, UK

L. Valentini
Department of Geosciences, University of Padua, Padua, Italy

F. Zunino
Laboratory of Construction Materials, École Polytechnique Fédérale de Lausanne, Lausanne, Switzerland

A. Alujas Diaz
Centro de Estudios de Química Aplicada, Universidad Central de Las Villas, Santa Clara, Cuba

Current developments towards low carbon cements have spurred the introduction of calcined clays for use as SCMs [1–3]. To suit exploration and extraction purposes, there is a need to extend the cement producer's toolbox with reliable and informative characterization techniques, robust towards the natural diversity and complexity of common and impure clays [4–6].

Clays have always been tedious materials to characterize in terms of composition and microstructure. The, by definition, fine-grained nature of clays and their mineralogical complexity made it difficult to study them using classical geological tools, such as optical microscopy. It was mainly the introduction of X-ray powder diffraction that led to the development of clay mineralogy [7, 8]. Complemented by chemical analysis, thermogravimetric analysis and spectroscopic techniques, and combined with powerful computational tools, clay mineralogists are now able to quantitatively determine the mineralogical make-up of clays to an unprecedented level of detail. Outstanding exploits of analytical prowess are featured in the so-called Reynold's Cup, a bi-annual global contest in quantitative mineralogical analysis of clays, where laureates succeed in accurately analysing challenging synthetic clay samples comprising up to 30 different mineral phases [9, 10].

Recent advances in clay mineralogical analysis were mainly driven by extractive industries. In particular, oil and gas exploration has exploited the complex and characteristic mineralogy of clays as a fingerprint for decoding reservoir rock sequences or hydrocarbon source rock maturity [11]. Other industries have focused on more accessible characteristics such as bulk chemical composition or colour to define acceptance criteria. Recent work has shown that the reactivity and performance of calcined clays as SCM depend strongly on the mineralogical composition of the raw clay, and that low grade kaolinitic (30–40 wt.% kaolinite) and other common, impure clays can also show acceptable cementitious properties after calcination [12–16]. Whilst several key texts exist for specific techniques and clay characterisation in a broad sense (these will be referenced throughout), these are largely application-agnostic—a treatment for the most relevant techniques specific to clays as SCMs is currently lacking. As such, this paper introduces key characterisation techniques for detailed clay mineralogy analysis for the specific application of producing

SCMs. X-ray diffraction, thermal analysis, and infrared spectroscopy are selected as common techniques available in most resource or material characterisation laboratories. These are discussed in terms of obtainable information, practical implementation, and analysis and interpretation related to clays. Although, complementary information with relevance to sampling and chemical analysis of clays are elaborated first.

2 Sampling and pre-treatment of raw clays

While the accuracy of modern analytical equipment is usually considered as the main source of variation in materials characterization, this may not be true in many cases. If not properly executed, sampling and sample preparation is a major source of variation and bias. For minerals that occur in such diverse and heterogeneous environments such as clay minerals, a representative sampling and an adequate understanding of the characteristics of the clay deposit are of paramount importance. Any conclusions that may be derived from state-of-the-art characterization techniques are not particularly meaningful unless one is certain that the sample is truly representative of the clay deposit that is intended to be characterized. The final goal of any sampling should be to provide the analyst with a homogeneous sample, representative of the lithological feature of interest at the predefined spatial resolution.

A geological evaluation of a clay deposit aims to provide more detailed information about the area of interest and raise confidence for industrial exploitation, moving from hypothetical resources to proven reserves. In a geological survey a grid of sampling points should be established, adapted to geomorphology and covering all relevant lithologies. A record should be made for every collected sample, including lithological and textural descriptions. A spatial mapping of the occurring lithologies is essential, as this provides indispensable information for resource volume estimations. The relevance of this information should not be underestimated, as this supports the interpretation of sample characterization results. Subsequent blending and homogenization of several samples together may reduce the resolution of the field observations [17].

As a rule of thumb, the higher the heterogeneity of a clay deposit, the more sampling points are required to obtain a representative averaged sample. All relevant lithologies present in a clay deposit should be representatively sampled in more than one location. For common manual procedures, such as shovelling or use of a hand auger, the surface should be cleaned before sampling to remove soil or surface alterations and avoid cross-contamination between different lithologies. Composite samples, representative of large areas, are generated by alternative sub-sampling of primary samples, taking several small portions of approximately the same size from each individual sample. Afterwards, pre-homogenization of composite samples is usually done by manual mixing procedures. Samples should be stored in well-marked sturdy containers or bags to avoid accidental mixing or spillage of materials, and mitigate moisture loss [17, 18].

Once clay samples arrive at the characterization facilities, they should be oven-dried at 105 °C to remove moisture and make the material easier to handle and comminute. At the same time, the moisture content of the clay can be measured. If the sample contains big chunks of clay it is recommended to manually reduce them to cm-size before drying, otherwise moisture may be trapped inside. A second step involves sample reduction up to approximately 1 mm. This step, usually done by jaw crushers, disk mills or similar tools, is essential to guarantee further success in homogenization and sample dividing steps. Coarse particles often have a somewhat different composition than finer fractions, and may not get evenly distributed during sample splitting. The use of high energy grinding or milling tools, such as planetary ball mills, is not recommended at this stage, as it may cause undesirable structural changes to the clay minerals in the sample. In addition, care should be taken to prevent dust losses during size reduction, otherwise the finest fraction could be underrepresented in the final sample. Final steps in sample preparation involve homogenization and further division and reduction of sample size. This could be done by manual (cone and quartering, sample splitters) or automated procedures (rotating and rotary tube sample dividers). If available, the use of automated procedures is recommended to reduce human bias [19].

Further steps regarding sample preparation for instrumental analysis, which usually involves grinding to analytical fineness, separation of fine fractions, or sample digestion, are specific for each analytical

technique and will be discussed separately in the following sections.

3 Characterisation techniques for qualitative and quantitative analysis

3.1 Chemical analysis techniques

Determining elemental composition is a key part of characterisation that can inform and help interpretation of other analytical techniques, as well as having specific value in its own right. Although clays and associated minerals are structurally complex materials, chemical analysis of its major components could be narrowed down to just a few elements: Si, Al, Fe, Mg, Ca, Na, K, Ti, Mn, S, P, and Loss on Ignition (LOI) evolved above 105 °C. This range of chemical elements could be assessed by most of the existing techniques, including standard methodologies involving wet chemistry methods. However, due to its increased availability, accuracy and faster sample processing, it is not infrequent that instrumental techniques such as X-ray Fluorescence (XRF), Atomic Absorption Spectroscopy (AAS) or Inductively Coupled Plasma—Optical Emission Spectrometry (ICP-OES) are used for routine chemical analysis in both industrial and research laboratories. Acknowledging that a plethora of other techniques are available, a brief overview of XRF and ICP-OES is given here, as these techniques are considered most relevant in the context of clay resource evaluation.

X-ray fluorescence (XRF) spectroscopy measures the characteristic energy (or wavelength) of X-ray photons (fluorescence). This fluorescence is emitted when a higher energy electron makes a transition to fill an inner shell vacancy, generated by the excitation of an inner shell electron by incident X-radiation [20]. The fluorescence is measured and recalculated into element (or oxide) concentrations. Laboratory-based XRF is a routine technique for mineral resource characterisation, usually conducted alongside XRD. Sample preparation is key to obtaining reliable XRF results. The main options for sample preparation are loose powders, pressed pellets and fused beads. Loose powders and pressed pellets are more easy to prepare, however are less accurate and sensitive due to matrix effects (i.e. the influence of neighbouring atoms in crystal structures on the measured energy spectrum [21]). Matrix effects are reduced when fused beads are made by thermal melting the sample using a fluxing material such as lithium metaborate. It is important to note that lighter and volatile elements (Na etc.) evaporate during the preparation and cannot be measured this way [22]. In order to adjust for matrix effects, it is recommend to generate a calibration curve using matrix-matched standards prepared in the same way as the samples for measurement.

Recent developments of most interest have been in handheld or portable XRF (pXRF). More details on pXRF instrumentation can be found elsewhere [20, 23, 24]. pXRF is truly portable, with handheld devices that can produce a reading within a few minutes. It has extensively been applied to detection of heavy metals in contaminated soils [25], but is also used in geochemical prospecting [26] and measuring the SiO_2:Al_2O_3 ratio in soils [27, 28]. Drawbacks from in-field pXRF are reduced accuracy, largely due to particle size and moisture content [25], with less effective detection for lighter elements [20]. Nonetheless, pXRF has the potential to increase the flexibility and reduce costs of clay prospecting by giving fast, in-situ measurements of key composition ratios.

Inductively coupled plasma optical emission spectroscopy (ICP-OES, also named ICP-AES, standing for *atomic* emission spectroscopy) provides the bulk chemical composition of a solution, converted in aerosol by means of a nebuliser and interacting with an argon plasma (5000–7000 K) that breaks the aerosol sample into atoms and ions in an excited state [29]. As the system returns to a lower energy state, radiation with a characteristic wavelength is emitted. The wavelength and intensity of the emitted radiation depend on the chemical species present in the sample, and their concentration. Quantification of the atomic species is obtained with the aid of calibrating solutions of known concentrations [30].

When compared to XRF, ICP-OES provides better accuracy and sensitivity, particularly for elements with low atomic numbers having low fluorescence yield. However, sample preparation is demanding, as it requires the digestion (dissolution) of the solid sample in a solution [31]. Incomplete sample dissolution is a common issue generating bias in the measurement, particularly in the case of certain stable silicates (e.g. zircon) and oxides (e.g. rutile). For clays, common digestion techniques comprise microwave assisted acid dissolution in which a

combination of acids is used (e.g. concentrated HBF_4, HNO_3 and HCl), or high temperature fusion with lithium metaborate followed by dissolution of the resulting beads into nitric acid. As in case of preparation of fused beads for XRF, volatile anions (SO_3, Cl, F,…) and alkali cations (Na, K,…) can be evaporated to a significant extent during high temperature treatment. For these elements, acid digestion at low temperature followed by anion chromatography or atomic absorption spectroscopy measurements provide more accurate determinations.

Low detection limits make this technique suitable for the analysis of contaminants in soil samples, although last-generation XRF instruments proved reliable in providing comparable accuracies in the chemical analysis of soils [32]. For heavy metal trace element analysis at the ppb level, ICP-mass spectrometry (MS) is the reference. ICP-OES can be considered as the preferred method for studying dissolution pathways of clay minerals used as SCM [33], rather than for prospecting purposes.

3.2 X-ray powder diffraction

X-ray powder diffraction is based on the interaction of X-rays that are scattered (also called reflected) by crystal lattice planes.[1] Unlike XRF, XRD relies the interference of elastically scattered X-rays, this means the detected X-rays have the same energy and wavelength as the source X-rays. Due to their very small crystal size and complex crystal structures clay minerals are one of the most difficult types of minerals to study. As a technique, X-ray diffraction (XRD) is regarded as one of the most informative and important experimental techniques with relevance to the mineralogical analysis of clays to date, providing insights hardly obtainable by other techniques [8]. XRD may even considered as indispensable when it comes to accurate qualitative and quantitative clay analysis, and is a core instrument in any clay mineralogy laboratory [34]. Invariably XRD has been the primary analysis technique employed by the best performing participants in the Reynolds Cup, a bi-annual contest in quantitative mineral analysis, with other techniques providing complementary, yet valuable information [9].

Nevertheless, extracting accurate and detailed information from XRD measurements on clays is not straightforward. It requires rigorous preparation techniques and careful analyses to distinguish and identify clay minerals. More than for any other technique, specific sample preparation routines and quantification approaches have been developed for XRD analysis of clays. In this respect, the advent of ever more powerful computerized analysis in the last decades has revolutionized the field by enabling structural simulations and accurate quantification of clay-bearing samples. This section presents a succinct and selective introduction to the topic, providing the reader with an overview of the methodology, where relevant illustrated by examples from case studies. For more advanced and complete treatises on the topic the interested reader is referred to Brindley and Brown [7], Moore and Reynolds [8] and Srodon [11].

3.2.1 Sample preparation and data collection

Sample preparation is of paramount importance with regards to correct identification of clay minerals and quantitative phase analysis of clays. The neglect of oriented samples treated at different conditions has been identified as one of the major error sources in quantitative phase analysis by analyses of participant performance in the Reynolds Cup [9]. The different pre-treatments and procedures to gain specific sample fractions are extensively described by Jackson [35], while Brindley and Brown [7] or Moore and Reynolds [8] provide comprehensive instructions for routine analysis. The US Geological Survey describes the different sample preparation techniques in an illustrated laboratory manual [36]. Regarding the aim of the sample preparation, a distinction has to be made between oriented mounts of the clay-sized fraction for the qualitative analysis of the clay minerals and a randomly oriented powder specimen of the bulk sample for quantitative analysis.

In order to retrieve a bulk powder, a representative clay sample has to be crushed and ground. There are two requirements for the sample: a particle size below 20 μm (best 5–10 μm [8]) and random orientation [37]. To achieve the former, hand grinding is unsuitable in most cases, while dry grinding in ball or disc

[1] These sets of parallel planes are usually referred to by their (hkl) or Miller indices. 1/h, 1/k and 1/l define the intercepts of the planes with the a, b and c dimensions of the unit cell, respectively (e.g. (00l) reflections are parallel to the a-b basal plane).

mills can easily overgrind the clay particles. The best results are reported to be achieved using a McCrone micronizing mill [8, 37]. Random orientation is another challenging task, as phyllosilicates tend to arrange in (00l)-direction. Even though preferred orientation can be reduced by using a side-loading technique, perfect randomness can only be achieved by spray drying [38], which is, however, no commonly available laboratory technique.

Particle-size separation is usually required to obtain the pure clay-sized fraction. Grinding in advance should be avoided, as thereby the clay-sized fraction gets enriched by non-clay minerals [39]. The disaggregation procedure strongly depends on the host rock. For a successful fractionation, the clay minerals need to be liberated while coagulation has to be prevented [40]. This can be achieved by dispersing the suspended sample with a small amount (< 0.5 wt.% [36]) of dispersant (e.g. sodium pyrophosphate [8]) using an ultrasonic probe. Chemical treatments may be necessary, in order to remove organics, carbonates, sulfates or iron oxides [35]. The XRD analysis of smectite rich clays is influenced by the type of interlayer cation and can thus require homo-ionic exchange. This can be achieved by treating the clay with a chloride solution of the corresponding cation, for example Li-exchange is used to distinguish montmorillonite from other smectites [40]. Size fractionation is carried out according to Stoke's law, using the different settling times depending on the particle size, which is calculated as equivalent spherical radius. The procedure can be accelerated by centrifugation. While the < 2 µm fraction is commonly used to prepare the oriented mounts, also the < 0.2 µm fraction can be of interest in some cases, for instance to distinguish illite–smectite mixed layers (see 3.2.2).

The clay-sized dispersions are afterwards transferred to oriented mounts and measured in air-dried condition. The easiest approach is to drip the suspension on a glass slide and let it dry. More sophisticated methods, which improve diffraction intensities, are found in the literature [8]. Treatment of the oriented mounts in an ethylene glycol (EG) saturated atmosphere at 60 °C allows the differentiation of swellable 2:1 clay minerals, as the d-values of the (00l)-reflections increase with EG solvation. A heat treatment of the mount at 550 °C helps to differentiate between kaolinite and chlorite [8].

Data collection by laboratory powder diffractometers should be performed over a wide enough angular range starting preferably at low angles in order to cover the typically high d-values for clay minerals. High peak-to-background ratio as well as sufficient counting statistics should be aimed for, in order to ensure proper data processing.

3.2.2 *Qualitative analysis*

The goal of qualitative XRD analysis is to correctly identify all minerals present. This list of identified minerals is the starting point for the next step of quantitative analysis, the more detailed the identification, the more accurate the quantification result.

As whole-rock mineral quantification is usually the goal, qualitative analysis usually starts on XRD measurements of the randomly oriented bulk sample [11]. Both non-clay and clay minerals can be identified based on routine peak searching and matching analyses with supplied databases (e.g. JCPDS) in common XRD analysis software. As an aid in identification Appendix 1 gives a search list containing *d*-values of the strongest reflection lines of common clay minerals and associated phases. Due to significant peak overlap and unpredictable effects of preferred orientation, identification of clay minerals down to the individual mineral species is usually not possible. Instead, aggregated groups of clay minerals are usually distinguished, such as kaolins, comprising kaolinite, dickite, nacrite and halloysite, or dioctahedral Al-rich 2:1 clays and micas, including illite, smectite, mixed-layer illite–smectite, muscovite and pyrophyllite. In consequence, also the quantification is aggregated at the same group level. While this level of detail may be sufficient to obtain total contents of kaolins, no distinction is made between e.g. illite or smectite that are known to have a very different impact on material performance as SCM. In addition, confusion may result from peak overlap, for instance distinguishing kaolinite and chlorite is not straightforward (see Fig. 1). The lack of detailed clay analysis results in important knowledge gaps as regards the potential use as SCM of ubiquitous clay minerals such as mixed-layer illite–smectite.

Detailed analysis of a sample's clay mineralogy is conveniently made by XRD measurements of oriented aggregates of the < 2 µm and/or < 0.2 µm fraction. The orientation treatment strongly enhances the (00l)

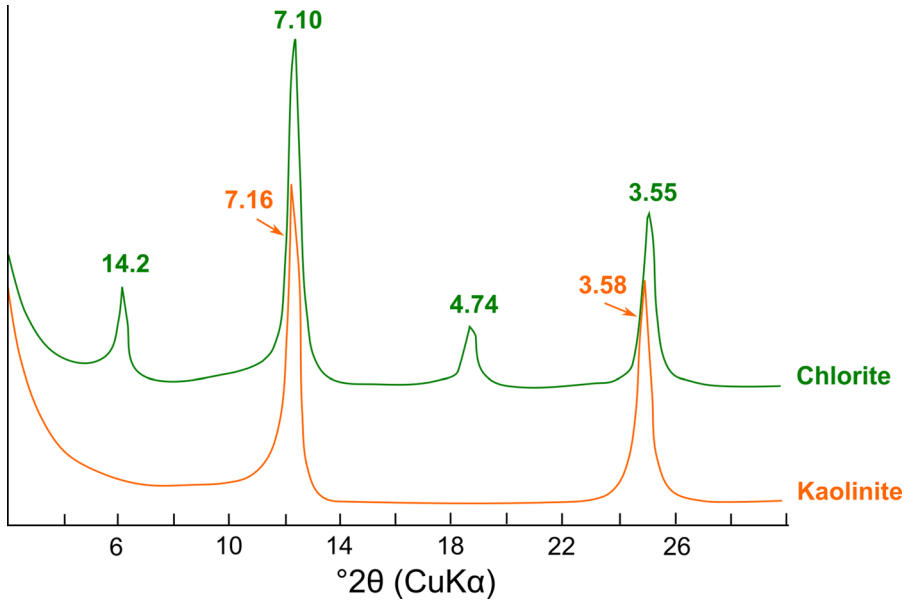

Fig. 1 XRD patterns of oriented mounts of chlorite and kaolinite illustrating strong overlap of the (00l) reflections

basal reflections of the clay minerals. Sampling the clay size fraction removes non-clay minerals present in the sample to a large extent, as such simplifying further analysis. Regular, discrete clay minerals can be identified by their rational series of (00l) peaks, interspaced at regular 2θ intervals. Clay mineral peaks are characteristically broader than common non-clay minerals such as quartz or feldspars. Distinguishing the main clay mineral types on oriented mounts is straightforward. Kaolinite is recognized from its 7.16 Å and higher order reflections, illite from its 10 Å and higher order reflections, chlorite from its 14 Å and higher order reflections etc. (Figs. 1, 2). However, difficulties arise when peak overlap between different clay minerals occurs such as between chlorite and kaolinite (Fig. 1), or when mixed-layer clay minerals are present. To resolve this issue, additional treatments are applied to the oriented sections. For instance, kaolinite and chlorite can be distinguished by a heat treatment of 1 h at 550 °C, at which temperature kaolinite will be decomposed while swelling clays potentially obscuring the 14 Å chlorite (001) peak will be collapsed to 10 Å and the chlorite 14 Å peak will become better visible. Swelling clays, such as smectites, are more easily identified after ethylene glycol (EG) solvation treatment. As illustrated in Fig. 2 the main peak of smectite (in its Ca-form) shifts from 14–15 Å in the air-dried state to about 17 Å when solvated by EG treatment, non-swelling clays such as illite or chlorite are not affected by EG solvation.

Additional information can be gained from examining the (060) reflection in the randomly oriented bulk sample. The *b* lattice parameter is sensitive to the cation size and site occupancy in the octahedral sheet and is therefore useful to distinguish between di- and tri-octahedral clay types. Di-octahedral, Al-rich clay minerals such as kaolinite, montmorillonite and illite have (060) reflections from 1.490 to 1.499 Å. Tri-octahedral Mg-rich clay minerals such as biotite, chlorites or palygorskite have (060) reflections in the range of 1.530 to 1.560 Å (cf. Appendix 1).

Mixed-layer clay minerals can be recognized by irrationally spaced or aperiodic reflection series and variable (00l) peak widths (Fig. 2). Both peak positions and width are used to estimate the sequence and proportioning of the interlayered clay minerals by applying the Méring principle [41]. For instance in Fig. 2 the proportioning 50/50 between illite and smectite can be derived from the difference in peak

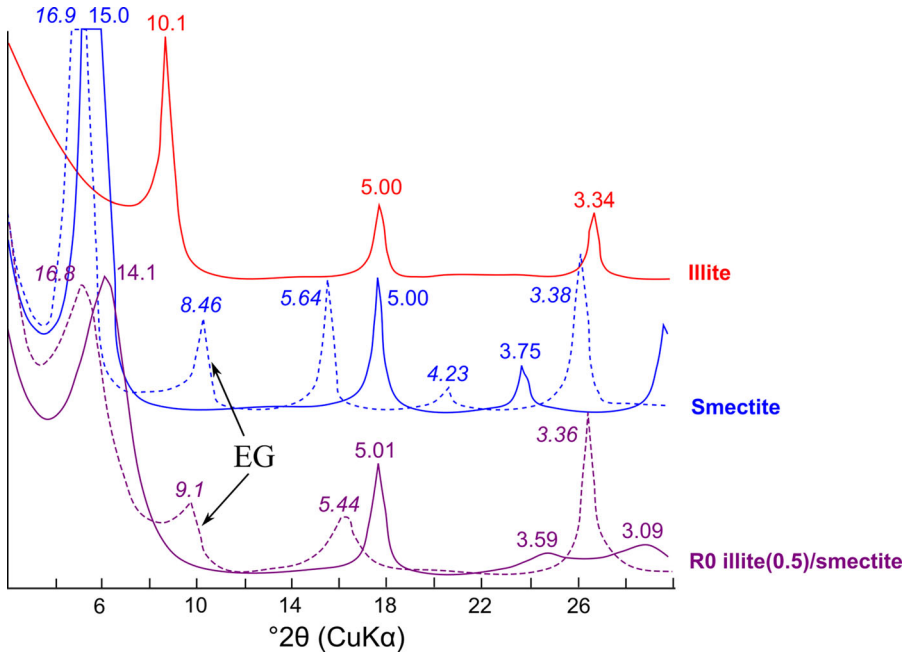

Fig. 2 XRD patterns of oriented mounts of illite, smectite and mixed-layer R0 illite(0.5)/smectite, the shift in basal reflections of the smectite clay minerals by ethylene glycol (EG) solvation is illustrated

position between the 001/002 (peak at 9.1 Å) and the 002/003 (peak at 5.44 Å) peaks of the EG solvated sample.

3.2.3 Quantitative analysis

Quantitative phase analysis (QPA) of raw clays by XRD is challenging because of the wide variety in chemical composition and crystalline structures, the occurrence of structural disorder such as interlayering or stacking disorder, and potential presence of amorphous phases [7, 11, 42].

QPA methods can be grouped in two categories: the first category includes those techniques aimed at quantifying the fraction of a given phase within a mixture, based on the intensity of a single reflection within the XRD pattern. The second category comprises *whole pattern methods*, by which quantification is achieved by fitting the full diffraction pattern.

Single reflection methods based on the addition of standards (internal standard methods) rely on removing the unknown mixture linear X-ray absorption coefficient from the equation that expresses the measured intensity of a given peak, relative to a given phase, to the volume fraction of that phase in the mixture [43]. The fraction of a crystalline phase within a mixture can be quantified by comparing the intensity of a selected reflection with that of a reflection of a standard phase. This phase can be added in known amount to the sample as internal standard, or separately measured as external standard. Internal standards should have low attenuation coefficients and few XRD reflections, possibly not overlapping with those of the phase to be quantified [7]. Care should be taken in homogeneously intermixing the sample with the standard. Typically, levels of 10 or 20 wt.% of internal standard are used, however higher levels may be preferable in certain cases. Common standard materials are corundum (α-Al_2O_3) and zincite (ZnO). Different versions of the internal standard method exist, mainly differing in the standard and the reference reflections of choice [44]. For example, the (113) reflection in corundum is used in the Reference Intensity Ratio (RIR) method [45]. In the external standard method, difference in the linear X-ray absorption coefficients of the sample and standard are mathematically accounted for, relying on accurate determinations of the sample and standard chemistry [46].

Single reflection methods often struggle with complex multicomponent materials that show broad and overlapping peaks, such as clays. Clay mineral peaks are often quite variable in peak width and intensity due to variations in microtexture, chemical composition and structure. Therefore, it is important to make calculations based on integrated peak intensities (peak area), rather than peak heights [47]. In addition, clay mineral reflections are often prone to preferred orientation (e.g. the 00*l* peaks). Such reflections should be avoided for accurate and reliable quantification. Single line reflections that are less sensitive to preferred orientation or variations in chemistry and structure, such as the above-mentioned (060) reflections for clay minerals, therefore need to be identified and calibrated for quantification purposes. The accuracy of single reflection methods can suffer significantly from peak overlap issues. This can be, to some extent, resolved by computationally fitting the whole observed pattern.

When it comes to whole pattern analysis, again two approaches are distinguished. In one approach, designated as "full pattern summation", the pattern is fitted by combining measurements of pure reference minerals that are pre-recorded on the same XRD instrument [48]. The scaling factors for each mineral are then recalculated to mass fractions using pre-determined conversion factors, in similar ways as for single-line reflections [10]. The advantage of full pattern summation methods is that there is no need to know the crystal structure of the clay mineral of interest. This can be advantageous in case of highly variable and defective clay structures such as mixed-layer clay minerals or smectites. The disadvantage is that pure or at least simple mixes of the mineral phase of interest need to be available and pre-recorded for each lab instrument that is used. It is important to note that the accuracy of this approach strongly depends on the selection and availability of appropriate mineral standards [10, 49]. Examples of software packages implementing the full pattern summation approach for clay analysis include FULLPAT [50], QUANTA® [51], RockJock [52], and PowdR [53, 54].

In the alternative approach, the pattern is fitted by theoretically calculated diffraction patterns using crystal structural and textural data in the Rietveld method. Rietveld quantification has as advantage that there is no need for building a library of pure reference patterns as diffraction patterns are calculated directly from crystallographic data and the diffractometer geometry [55]. The main drawback of Rietveld based methods is that they typically assume three dimensional periodicity, which is often not the case for clay minerals that show complex interstratification and defect crystal structures leading to strongly asymmetric peaks [56]. Specific software or software having extensions capable of dealing with interstratified clay minerals include Profex/Autoquan/BGMN [57, 58], and TOPAS/TOPAS-Academic [59, 60]. As these extensions may be somewhat computationally expensive, also hybrid approaches combining Rietveld for known, crystalline phases, with profile summation for Partially Or Not Known Crystal Structures (PONKCS) have been developed and successfully applied to quantitative XRD analysis of clays [61].

In the internal and external standard methods, the amorphous phase content is calculated as the difference between the sum of all crystalline phase mass fractions and 1. This fraction may also include contributions from non-identified minerals and misfits of the calibrated patterns or crystal structures and is therefore often referred to as "unknown and amorphous phase" fraction [62].

3.3 Thermal analysis

Thermal analysis is a general term that covers a variety of techniques that record physical and chemical changes occurring in a substance once it is subjected to changes in temperature. Four of these techniques, Thermogravimetric Analysis (TGA), Differential Thermal Analysis (DTA), Differential Scanning Calorimetry (DSC) and Loss on Ignition (LOI) have become powerful tools for qualitative and quantitative analysis of clays and clay minerals [63, 64]. In fact, clays were among the first materials investigated by thermal analysis, following the early development of these techniques at the end of the nineteenth century [65].

The International Confederation of Thermal Analysis (ICTA) defines DTA as a method that monitors the temperature difference between a sample and a thermally inert reference as a function of time and/or temperature. DTA therefore allows to detect exothermic and endothermic phenomena. A similar technique, DSC, records the energy associated to the exothermic or endothermic phenomena by applying and measuring power compensation to equalize

temperatures or by measuring the heat flux between the sample and the reference. For quantitative analysis, DSC is by principle superior to DTA since the former method not only registers the endothermic/exothermic effect but also allows direct measurement of its associated energy. However, the achievable upper temperature limit in DSC is often lower than that of DTA [66]. In contrast, TGA measures the change in mass of a material over a temperature range using a predetermined heating rate or as a function of time under an isothermal regime. This technique is very useful for monitoring phenomena associated to mass changes, such as decarbonation, dehydration, dehydroxylation, decomposition of sulfides/sulfates, combustion and oxidation reactions. By performing stoichiometric calculations, the registered mass changes can be used for quantitative purposes [67, 68].

Combination of TGA with DTA/DSC is increasingly available in modern thermal analysis instruments. In this combined analysis a temperature shift is usually observed between TGA and DTA/DSC curves for the same phenomena. This is because mass changes are detected almost instantaneously while the associated temperature changes are perceived with some time delay by DSC. The magnitude of this shift is dependent on experimental factors such as heating rate or the amount of analyzed sample. The best sample arrangement for TGA experiments is a thin layer of powdered sample that allows a swift release of decomposition gases, whereas the best one for DTA is the sample totally surrounding the thermocouple, to increase the efficiency of the thermal signal. Slow heating rates may favor resolution in TGA curves but decrease the intensity of the signal detected by DTA/DSC [63, 67, 69]. As both measurements cannot be made in their optimal configuration at the same time, compromise solutions are often used. Traditional thermal analysis techniques may also be complemented by evolved gas analysis methods (EGA), that through the use of FTIR, gas chromatography or mass spectrometry assist in the interpretation of the nature and the amount of the evolved products for a given reaction, such as H_2O, CO_2 or SO_2 [69].

3.3.1 Qualitative thermal analysis of clays

Upon heating of raw clays from room temperature to approximately 1000 °C, three phenomena can be clearly distinguish in thermal analysis curves: (1) dehydration (~ 50–300 °C, mass loss, endothermic), (2) dehydroxylation (~ 350–950 °C, mass loss, endothermic)) and (3) recrystallization (for temperatures > 900 °C, exothermic, no mass changes, only detected by DSC/DTA). While DTA/DSC are always represented as differential curves, where clearly visible peaks can be directly associated to the occurring transformations, TGA is depicted as a step-like curve, with a much lower resolution between consecutive thermal phenomena. Therefore, for accurate qualitative interpretation of TGA curves the use of the first derivative of the thermogravimetric curve (DTG) is strongly advised, which allows not only to improve resolution between adjacent thermal phenomena but also to detect small mass changes that may not be directly spotted from the regular thermogravimetric curve [68, 70].

Dehydration is the release of molecular water that may be adsorbed at the inner/outer surface of minerals or trapped within its pore or channel structure. Molecular water is also present in the interlayer region of most 2:1 clay minerals, associated to the cations positioned in the interlayer. For clay minerals, the magnitude and temperature range of the dehydration step depends on a large number of factors such as storage conditions, structure and crystallinity of the clay mineral, and nature and abundance of the cations in the interlayer region, among others [71, 72]. Dehydration is particularly useful to identify the presence of 2:1 clay minerals that exhibit strong dehydration effects, such as smectites, vermiculites or some micas, with typical mass losses that range from 7 to 17 wt.% in air dried samples [63, 68, 69]. However, it should be stress out that not only 2:1 clay minerals may exhibit significant dehydration steps, as this is also the case for halloysite (~ 12 wt.%), poorly crystallized kaolinites and some non-crystalline associated phases to 1:1 clay minerals, such as allophane and imogolite [67, 68].

The hydroxyls groups in the clay structure are much more strongly bonded than adsorbed or interlayer water and requires a higher temperature for its removal. Upon heating, hydroxyls are liberated over a broad temperature range related to their different locations within the clay mineral structure and their wide range in bond energy distribution. As a general rule, clay minerals with a higher level of structural disorder exhibit dehydroxylation effects at lower temperatures and within a wider temperature range

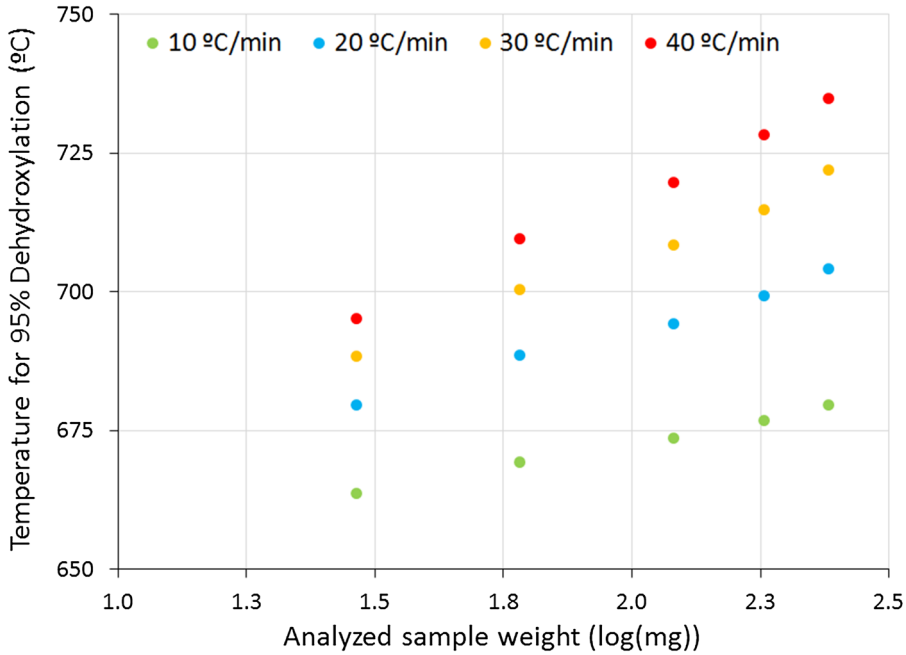

Fig. 3 Influence of heating rate and sample mass in dehydroxylation temperature of a kaolinite sample

compared to the same clay minerals with a higher crystallinity [71, 73, 74]. The nature of the cation bonded to the hydroxyl group also influences dehydroxylation temperature, as the bond energy increases according to the sequence Fe-OH < Al-OH < Mg-OH [63, 64]. The mass fraction that hydroxyls represent in the structural unit, their position in the crystal lattice as well as their average bond energy are characteristic to each individual clay mineral. Therefore, the temperature range, peak temperature, shape, and magnitude of the thermal effects associated to the dehydroxylation of clay minerals are of great analytical value for both qualitative and quantitative interpretation of clay samples.

Concerning sample characteristics, the temperature range and rate of dehydroxylation is mainly depending on the degree of structural disorder of the clay minerals, the size distribution of crystallites and physical particles, and the degree of packing [71, 73–75]. Due to heat diffusion effects, an increase in sample size or in heating rate will shift dehydroxylation temperatures to higher values, following a logarithmic law as observed in Fig. 3 for a natural kaolinite. In order to keep results comparable, linear heating rates of 10 °C/min and analysed sample masses of about 30–50 mg are usually recommended as experimental conditions in most modern equipment. As for furnace atmosphere or purge gas, air is the usual option, in case carbonation of oxidation needs to be avoided an inert atmosphere (nitrogen, argon) is preferable. Given the strong influence that experimental conditions and sample characteristics have on the dehydroxylation temperature range, there is a large scatter of temperature values reported in the scientific literature for similar clay minerals. An attempt is given in Table 1 to summarize the behaviour of selected clay minerals relevant as source of SCM. As noticed, although dehydroxylation may occur over a wide range of temperatures (grey temperature ranges in Table 2), for each group of clay minerals there is a relatively narrow temperature interval (black temperature ranges in Table 1) in which most of the dehydroxylation phenomena (> 90%) take place.

Finally, at temperatures above 900 °C, recrystallization takes place, indicating the conversion of structurally disordered, metastable phases to more stable, crystalline high-temperature phases. Common phases formed during recrystallization are mullite, cordierite, enstatite and cristobalite. Similar to dehydroxylation, the temperature, width and shape of the exothermic recrystallization peak depends on the type, crystallinity and amount of clay minerals present in the

Table 1 Temperature ranges for dehydroxylation of some representative clay minerals, data adapted from [63, 68]

	ΔOH^- (wt.%)	Clay mineral	Dehydroxylation temperature (°C) 300 400 500 600 700 800 900 1000
Kaolinite group	~ 14.0	Kaolinite	
		Dickite	
Smectite group	4.3 – 5.0	Nontronite	
		Montmorillonite	
True and brittle micas	4.5 – 5.3	Muscovite	
		Illite	

Table 2 Quantitative phase analysis results of the case study kaolinitic and smectitic clays as obtained by XRD-Rietveld refinement

Phase	Kaolinitic clay (mass%)	Smectitic clay (mass%)
Kaolinite	27.3	8.4
Illite/Muscovite	25.4	3.6
Montmorillonite	–	62.5
Quartz	41.0	14.2
Feldspar	2.3	4.7
Calcite	–	1.3
Rutile/Anatase	1.4	1.4
Iron oxides/hydroxides	1.5	
Amorphous/unknown phase	1.1	3.8

sample [63, 67, 76]. Identification of these three temperature ranges are amongst the most useful information (and easily obtained) for a potential SCM, as they inform the feasible range of calcination temperature for a given clay. Alongside the clay minerals themselves, TG curves can also be helpful in identifying associated minerals in clays and soils—particularly those which diffract weakly in XRD patterns (due to poor crystallinity and/or fine particle size) but exhibit distinctive mass loss behaviour, such as goethite [77].

3.3.2 *Quantitative analysis of clays based on TGA/DTG curves*

Quantitative analysis by TGA is based on the assumptions that, within a given temperature range, an individual mineral is solely responsible for the registered mass changes, that the registered reaction follows a known stoichiometry, and that chemical variability for the quantified mineral is low enough so that precise calculations based on the registered mass changes are possible. The accuracy is favoured for phases with a lower stoichiometric factor, i.e. with a lower ratio between its molar mass and the mass change associated to its decomposition reaction. Therefore, the accuracy of quantitative analysis based on TGA measurements is different for each mineral [63]. An important potential source of error is the overlap between decomposition reactions of the different clay and non-clay minerals present in the sample. In a best case scenario this only decreases the accuracy of the determination, however in unfavourable conditions this may totally obstruct the identification and quantification of individual minerals [68]. Finally, all quantitative results should be reported based on dry mass and not initial sample mass. Variable amounts of absorbed/adsorbed water in clay samples should not be taken into account in stoichiometric calculations.

The expression used to calculate the quantity of a given clay mineral based on its dehydroxylation reaction is:

$$\text{Clay mineral content} = \frac{100 * (\text{Mass}_{T1} - \text{Mass}_{T2})}{\text{Mass}_{Dry} * \Delta OH} \quad (1)$$

In Eq. 1 the difference (Mass T_1 Mass T_2) represents the mass loss over the dehydroxylation interval, with T1 and T2 being the lower and upper temperatures of the interval. Mass_{Dry} is the mass of the dry sample (usually at temperatures between 200 and 250 °C); while ΔOH is the mass fraction of the clay mineral represented by hydroxyl groups, without considering the variable content of absorbed/adsorbed water in the stoichiometric calculations. The value of ΔOH, expressed as mass percent, is ∼ 14 wt.% for 1:1 clay minerals and range from 4 to 5.5 wt.% for 2:1 clay minerals that show larger chemical and structural variability [78]. Different approaches can be followed to determine the mass loss associated to a given thermal phenomenon, the two most common being the tangent method in the TGA curve and the peak integration method in the DTG curve. Combined analysis is also quite suitable, by using the DTG curve to select temperature limits for the dehydroxylation effect and then calculating mass changes in the TGA curve using the previously defined temperature interval [69].

Although quantitative analysis by TGA is possible for all individual clay minerals, for complex mineralogical systems reliable quantification is mainly limited to members of the kaolinite group, characterized by a low variability in its chemical composition and a lower stoichiometric factor (∼ 7.2) in comparison to 2:1 clay minerals (∼ 19–23). Whilst quantitative analysis for clay minerals with variable composition can be attempted, this requires either an assumption of the stoichiometric formula [79] which reduces accuracy, or labour-intensive laboratory work to determine the exact formula of the clay mineral of interest (which is arguably not worth the effort involved). Some degree of overlap cannot be avoided between kaolinite dehydroxylation and decomposition of 2:1 clays or some non-clay minerals such as pyrite, alunite or poorly crystallized carbonates, all mineral phases that can be found naturally associated to kaolinite [74, 75]. Therefore, before starting qualitative or quantitative interpretation of thermal analysis, the gathering of additional information regarding the mineralogical composition of the analysed sample is strongly advised, either by using other characterization techniques such as XRD and FTIR; or by collecting information from literature. The identification of minerals that may overlap with the thermal dehydroxylation of clay minerals is of obvious importance. Once this is done, measurement bias can be minimized by carefully selecting the temperature range for determination of mass losses on the DTG curve, or by using a slower heating rate (yielding a higher sensitivity and a better resolution) to detect and distinguish smaller mass change events.

The above statements are illustrated in Fig. 4, where DTG curves for representative members of clay mineral groups commonly used as or associated to SCM source materials are shown together with the characteristic S-shaped curves that describe the degree of dehydroxylation under a linear heating rate of 10 °C/min. As can be observed, although dehydroxylation of kaolinite covers approximately the entire range between 350 and 800 °C, for practical purposes the upper limit for determining mass losses could be set to 650 °C, a temperature for which kaolinite has reached 95% degree of dehydroxylation and the overlap with the dehydroxylation of illite and montmorillonite is kept to a minimum. Finally, it should be stressed that in complex mineral mixtures it is almost impossible to distinguish by thermal analysis measurements between the different clay minerals of the kaolinite group, making it more correct to group results as a single value, denoted as equivalent kaolinite [80]. Similar reasoning also applies to complex mixtures of 2:1 minerals.

Because the above-mentioned phenomena may interfere to some extent with accurate determinations of clay minerals by TGA/DTG, it is always advisable to cross-check quantitative results obtained by thermal analysis with other analytical techniques. In general, good agreement has been reported when comparing XRD with TGA results for kaolinite group minerals, as depicted in Fig. 5, however there are few reports for 2:1 clay minerals. Major differences are expected for samples with low crystallinity, because clay minerals may be underestimated by XRD, while the trend in TGA may show a slight overestimation due to overlapping of thermal decomposition events of other

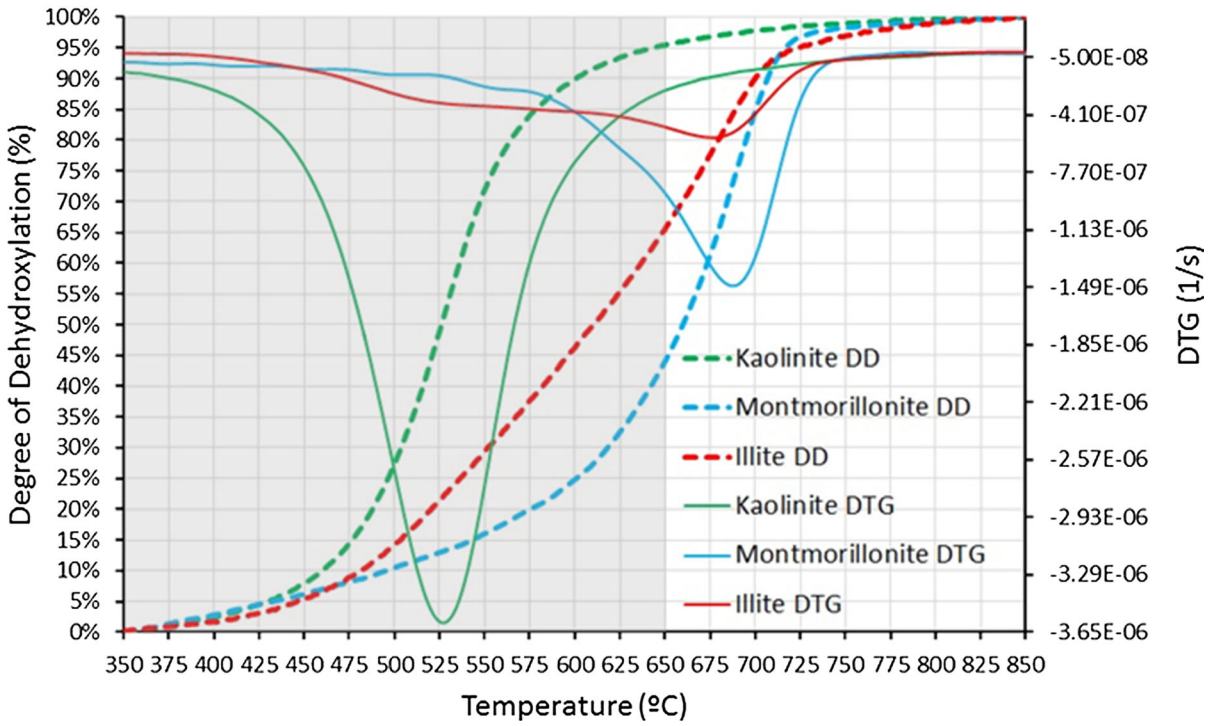

Fig. 4 Degree of dehydroxylation and DTG curves for kaolinite, montmorillonite and illite (heating rate 10 °C/min). Temperature limits selected for (equivalent) kaolinite quantification are indicated by the shadowed area

minerals. The chemical composition could be used to double check results from mineralogical analysis, especially for clay minerals with a low chemical variability. For example, for any given sample, kaolinite content should always be lower than the mass ratio Al_2O_3/0.395, corresponding to the chemical composition of kaolinite clay minerals [13].

3.3.3 Loss on Ignition

Loss on ignition (LOI) measurements are a well-known technique in the study of soils and minerals and also a useful way to characterise raw clays. The concept is similar to that of TGA except that the mass loss measurements are intermittent instead of continuous. LOI measurements are usually conducted by placing a few grams of crushed or powdered material in a muffle furnace at set temperatures (e.g., 200 °C, 550 °C, 950 °C, 1050 °C) and the mass loss recorded over each interval. LOI measurement has the advantage over TGA in that it does not require sophisticated equipment and is quite straightforward to be carried out. Another major difference between LOI and TGA is that there is less control of the atmosphere for LOI measurements as these are usually done without a purge gas. LOI can be a valuable indicator for the presence of certain minerals as well as to test the variability/consistency of the raw clays. LOI tests may be used for quality control of clay—for example, ASTM C311/C311 M—13 instructs for natural pozzolans (including calcined clays) to be 'ignited to constant mass' at 750 ± 50 °C, with a maximum allowable LOI of 10%. For kaolinitic clays, the kaolinite content may be estimated from the mass difference recorded after heating to 400 and 600 °C [81]. However, such tests may also fail to provide correct assessment in case more than one mineral loses mass over the targeted temperature range [81]; for example, calcite [82], which can be found in soils.

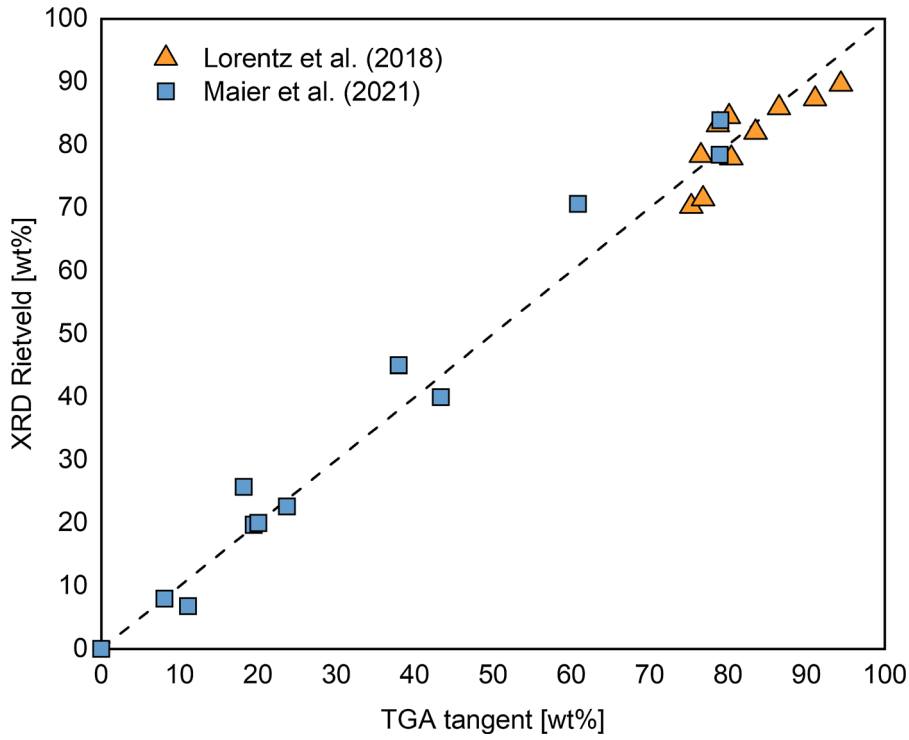

Fig. 5 Comparison of kaolinite content determined by XRD and TGA, data from [13, 4]

3.4 Vibrational spectroscopy

3.4.1 Infrared spectroscopy

Infrared spectroscopy was introduced in the middle of the twentieth century to study the bond structures of solid, liquid, and gaseous molecules. IR spectroscopy involves measuring the resonance between IR photons and the vibrational energy of molecular bonds [83], and the instrumentation is commonly used in three subranges: near- (12,500–4000 cm^{-1}), mid- (4000–400 cm^{-1}), and far-IR (400–10 cm^{-1}). When infrared radiation is sent through the sample part of the energy spectrum is absorbed to cause the excitation (stretching, rotation, and bending) of specific bonds in the molecules. The frequency, intensity, and width of the absorbance signal obtained depend on the sample's local structure, composition, and microstructure. Every molecule has a unique IR fingerprint, making IR-spectroscopy an invaluable technique to identify minerals, especially in clay science [84].

3.4.1.1 MIR for clay minerals identification In this section, the focus is on the interpretation of mid infrared (MIR) absorbance spectra for clay characterization. In this case, sample preparation requires careful intergrinding of 1 wt.% of raw clay with KBr powder[2] to avoid crystalline alteration. The resulting powder is subsequently pelletized under load. The pellet can be kept in an oven at 105 °C for extended periods to avoid or remove absorbed moisture. A standardized procedure for pellet preparation is critical for obtaining consistent and comparable FTIR spectra for clay identification [85].

For clay minerals, the characteristic absorption bands present in the MIR range (4000–400 cm^{-1}) are associated mainly with stretching and bending vibrations O–H and Si–O bonds, and Al–O, Fe–O and Mg-O bonds. According to the clay mineral structure (OH groups coordinated with octahedral atoms, the interlayers cations, surrounding tetrahedral lattice), the absorbed energies at different wavenumber have a typical molecular spectrum. A recent review of IR-spectra of clay minerals is published by Madejová

[2] KBr is hygroscopic and should be dried and kept dry before measurement in order to avoid detecting diffuse water signals in the measurement.

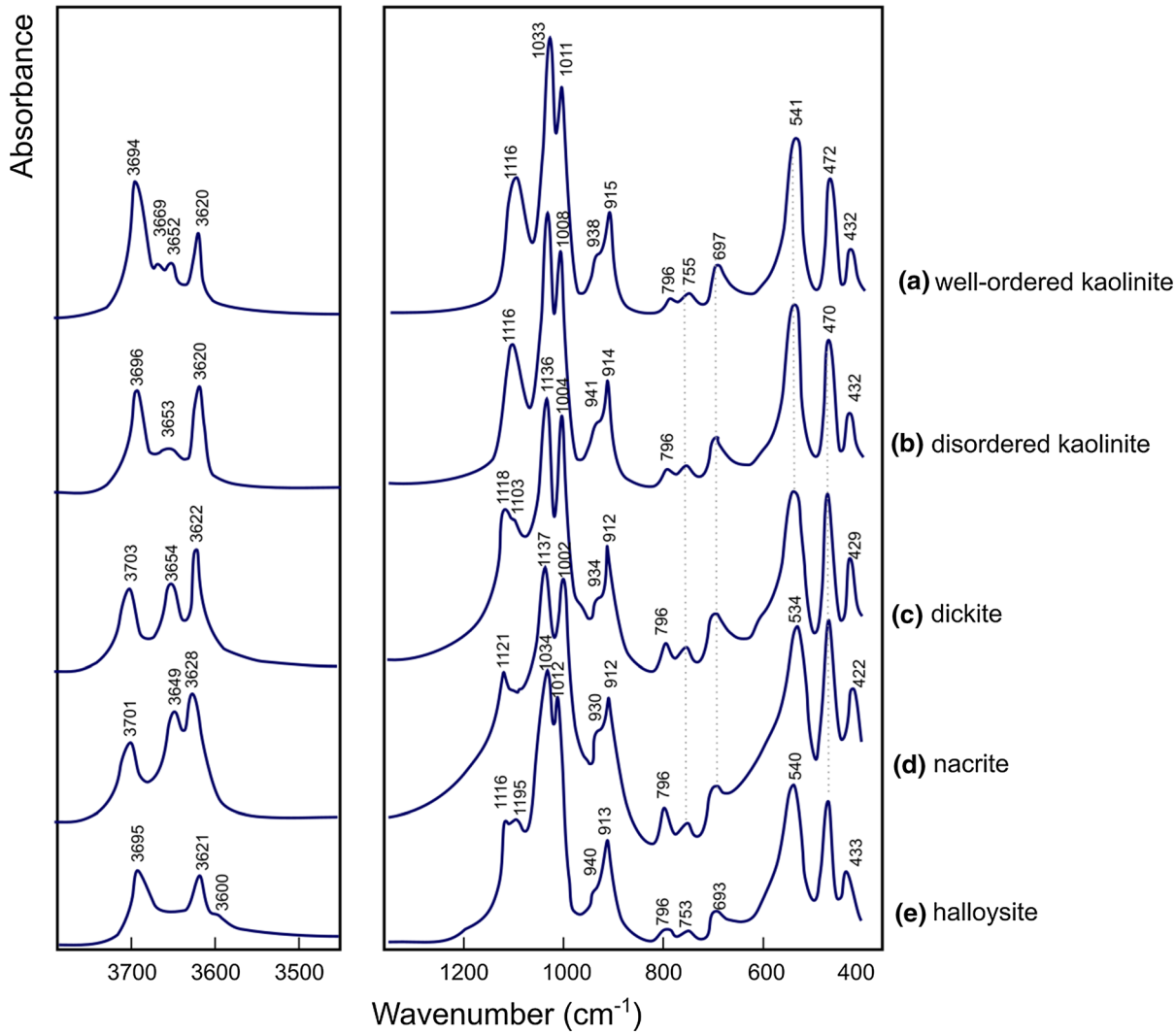

Fig. 6 MIR spectra for 1:1 clay minerals: **a** well-ordered kaolinite; **b** disordered kaolinite; **c** dickite; **d** nacrite, and **e** halloysite (adapted from [86])

et al. [86]. The main bands for identification clay minerals in common clays are listed in Appendix 2. Whilst MIR spectroscopy is predominantly a laboratory-based technique, portable handheld instruments have now entered the market—a previous study has shown comparable performance to desktop instruments in the characterisation of soils [87]. Such advances in instrumentation could help open up MIR spectroscopy as a rapid, on-site technique for clay prospecting (Fig. 6).

3.4.1.2 1:1 clay minerals—kaolins Figure 6 shows the FTIR spectra of 1:1 clay obtained from Madejova et al. [86] as an example. In the OH stretching region (3600–3700 cm^{-1}), ordered kaolinite (Fig. 6a) shows four bands at 3694, 3669, 3652, and 3620 cm^{-1} [88–91]. The 3620 cm^{-1} band is attributed to the stretching vibrations of inner OH- bonded to octahedral cations, and the other bands are due to coupled stretching vibrations of OH groups located at the surface of the dioctahedral sheet of the layers. The 3694 cm^{-1} band corresponds to the in-phase coupled stretching vibration of surface-perpendicular-OH,

whereas the 3669 and 3652 cm^{-1} bands are due to out-of-phase coupled vibrations of these groups [88, 89]. For disordered kaolinite (Fig. 6b), the bands at 3620 and 3694 cm^{-1} remain, while a single band replaces the doublet of 3669 and 3652 cm^{-1} at 3653 cm^{-1} [92]. The P0 index measures the crystallinity, which is calculated as the intensity ratio of the bands at 3620 cm^{-1} and 3694 cm^{-1} [91]. P0 > 1 reveals an ordered structure, and P0 < 1 indicates a disordered structure. The P0 index can be affected by the presence of illite, quartz, or feldspars [92].

In the OH- regions, the dickite spectrum shows three absorption bands at 3703, 3654, and 3622 cm^{-1} (Fig. 6c) (Balan et al., 2010). The 3623 cm^{-1} band is assigned to the inner OH, the 3710 cm^{-1} band to the inner-surface OH, and the 3656 cm^{-1} band to the remaining OH groups. Nacrite (Fig. 6d) shows similar OH- stretching bands to those of dickite in this region. Halloysite (Fig. 6e) shows two prominent bands at 3695 cm^{-1} and 3621 cm^{-1} in the OH stretching region, while two weak intermediate bands could be found in prismatic tubular halloysite [93].

In the 1400–400 cm^{-1} region (Fig. 6), the spectra of 1:1 kaolin-group clay minerals are similar, showing a strong and sharp band in the 1120–1000 cm^{-1} region assigned to the Si–O stretching vibrations, two strong bands at 1037–1033 cm^{-1} and 1012–1002 cm^{-1} attributed to the Si–O–Si stretching vibrations, and around to 1100 cm^{-1} due to Si–O bond stretching. At 470–472 cm^{-1}, the bending vibrations Si–O–Si groups are displayed. Related to alumina bonds, the bending vibration of Al_2OH bands appears near 915 and 935 cm^{-1}, the bending vibrations of Si–O–Al^{VI} near 540 cm^{-1} [94].

3.4.1.3 2:1 layer clay minerals: smectites, illite and muscovite The most common 2:1 layer-type clay minerals include smectites, illites, and micas. Smectites and micas are usually classified as dioctahedral and trioctahedral. In the smectite, the negative charge on the layers is balanced by hydrated exchangeable cations in the interlayer space or surface. On the contrary, no hydrated cation occupies the interlayer spaces in the illites and micas.

For smectites (Fig. 7a–c), the OH- stretching region shows a broad band in the 3620–3650 cm^{-1} range assigned to the OH groups coordinated to different octahedral cations, mainly Al_2OH, AlMgOH, and $AlFe^{3+}OH$. In smectites dominated by tetrahedral substitution (e.g. Si by Al in beidellite), the OH^- bands appear at higher wavenumbers (3652 and 3623 cm^{-1}) than those dominated by octahedral substitution (e.g. Al by Mg in montmorillonite) with a band at 3623 cm^{-1}.

The OH bending region (950–800 cm^{-1}) is more sensitive to the occupancy of the octahedral sheets: the bands at 924 cm^{-1} assigned to (Al_2OH) and at 863 cm^{-1} assigned to AlMgOH are shown in the spectrum of beidellite (Fig. 7a). For montmorillonite (Fig. 7c), the band at 880 cm^{-1} is assigned to $AlFe^{3+}OH$. In the Si–O stretching region, smectites show a broad band assigned to Si–O–Si stretching vibrations (1070–970 cm^{-1}) and perpendicular Si–O vibration near 1100 cm^{-1} [94].

Figure 7d presents an IR spectrum of illite. In the OH stretching region, a single band is apparent at 3623 cm^{-1}. In the 1400–400 cm^{-1} region, the bands around 1043 cm^{-1} are assigned to Si–O stretching vibrations. The (Al_2OH) band at 916 cm^{-1} is similar to those found for montmorillonites. A weak band at 831 cm^{-1} of illites is assigned to octahedral AlMgOH bending vibration or Al^{IV}–O vibration out of plane, and the 756 cm^{-1} band to Al–O–Si vibration [94]. The 801 and 780 cm^{-1} doublet is characteristic for quartz present in the sample.

For muscovite (Fig. 7e), the spectrum shows OH stretching vibrations at 3627 cm^{-1}, a shoulder near 3659 cm^{-1} related to OH groups close to AlO_4 tetrahedron, and a band at 3627 cm^{-1} assigned to OH groups bonded with neighbouring SiO_4 tetrahedra. The Si–O stretching and OH bending vibrations appear as broad bands (1028 and 933 cm^{-1}). Also, tetrahedral substitution generates bands at 831 and 753 cm^{-1} are attributed to the vibration of Al^{IV}–O and Al^{IV}–O–Si, respectively. The 524 cm^{-1} band is due to Al^{VI}–O–Si bending vibrations, and both 472 and 428 cm^{-1} bands are assigned to Si–O–Si bending vibrations.

3.4.1.4 2:1:1 clay minerals: chlorites In case of chlorites the crystal structure is formed by a regular stacked 2:1 layers separated by a brucite-like interlayer. FTIR spectra of chlorites include the stretching vibration bands of OH groups from both the 2:1 layer and the hydroxide sheet that occupies the interlayer [92]. For example, clinochlore (Fig. 7f) shows a broad band at 3628 cm^{-1} with a weak inflection near 3680 cm^{-1} and a wide shoulder centred

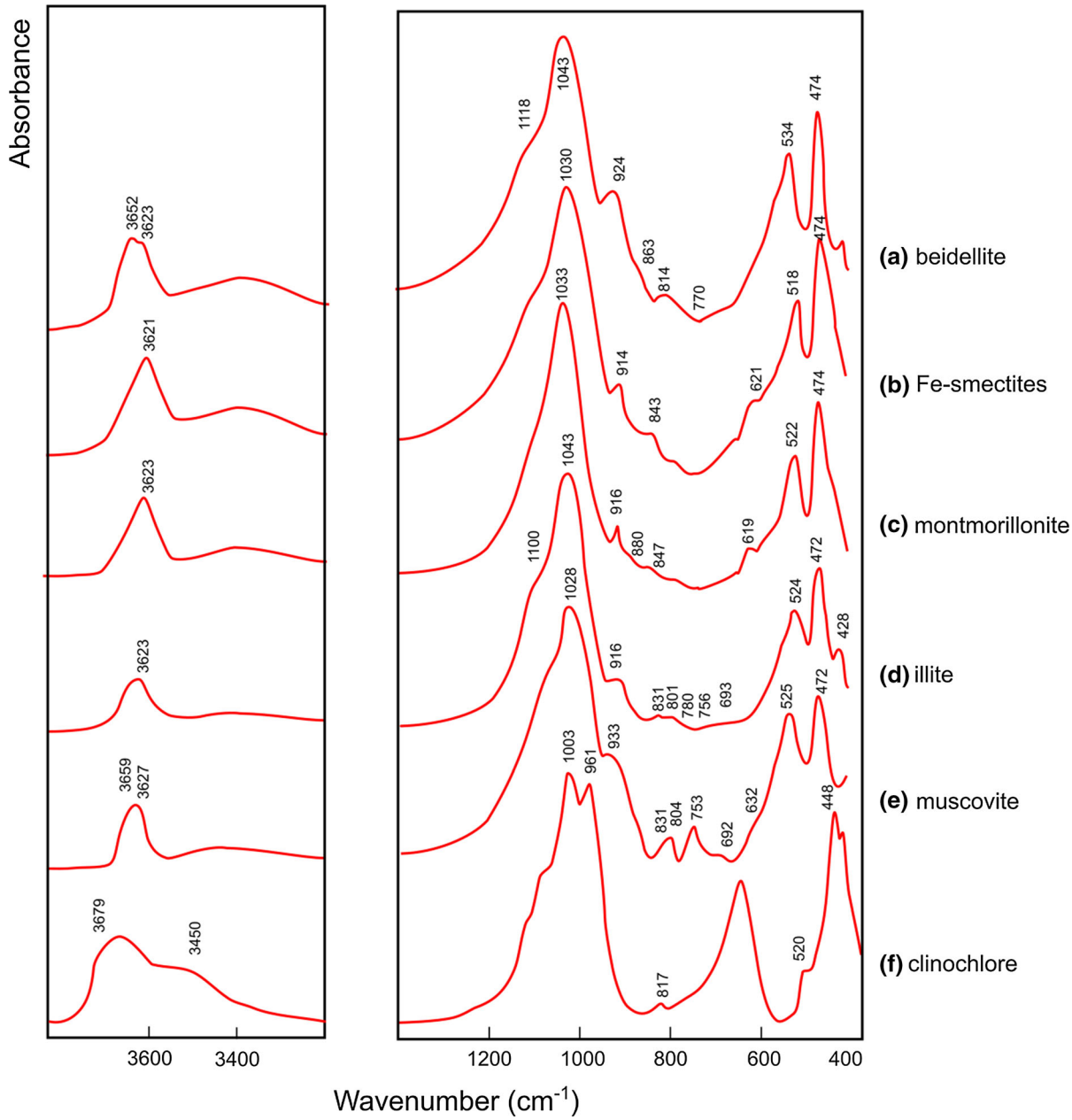

Fig. 7 MIR spectra for layer minerals: **a** beidellite, **b** Fe-smectite; **c** montmorillionite; **d** illite and **e** muscovite (selected and adapted from [86])

near 3450 cm^{-1}. The bands at 3628 and 3450 cm^{-1} are assigned to the OH stretching vibrations of the interlayer, and the absorption band near 3680 cm^{-1} is related to the Mg-OH stretching vibration in the trioctahedral 2:1 layer [86]. In the Si–O stretching region, clinochlore shows a splitting Si–O band (1003 and 961 cm^{-1}), and the band at 820 cm^{-1} is assigned to the Al–O vibrations. The bands assigned to OH bending vibrations at 700–600 cm^{-1} are strong in chlorites [92].

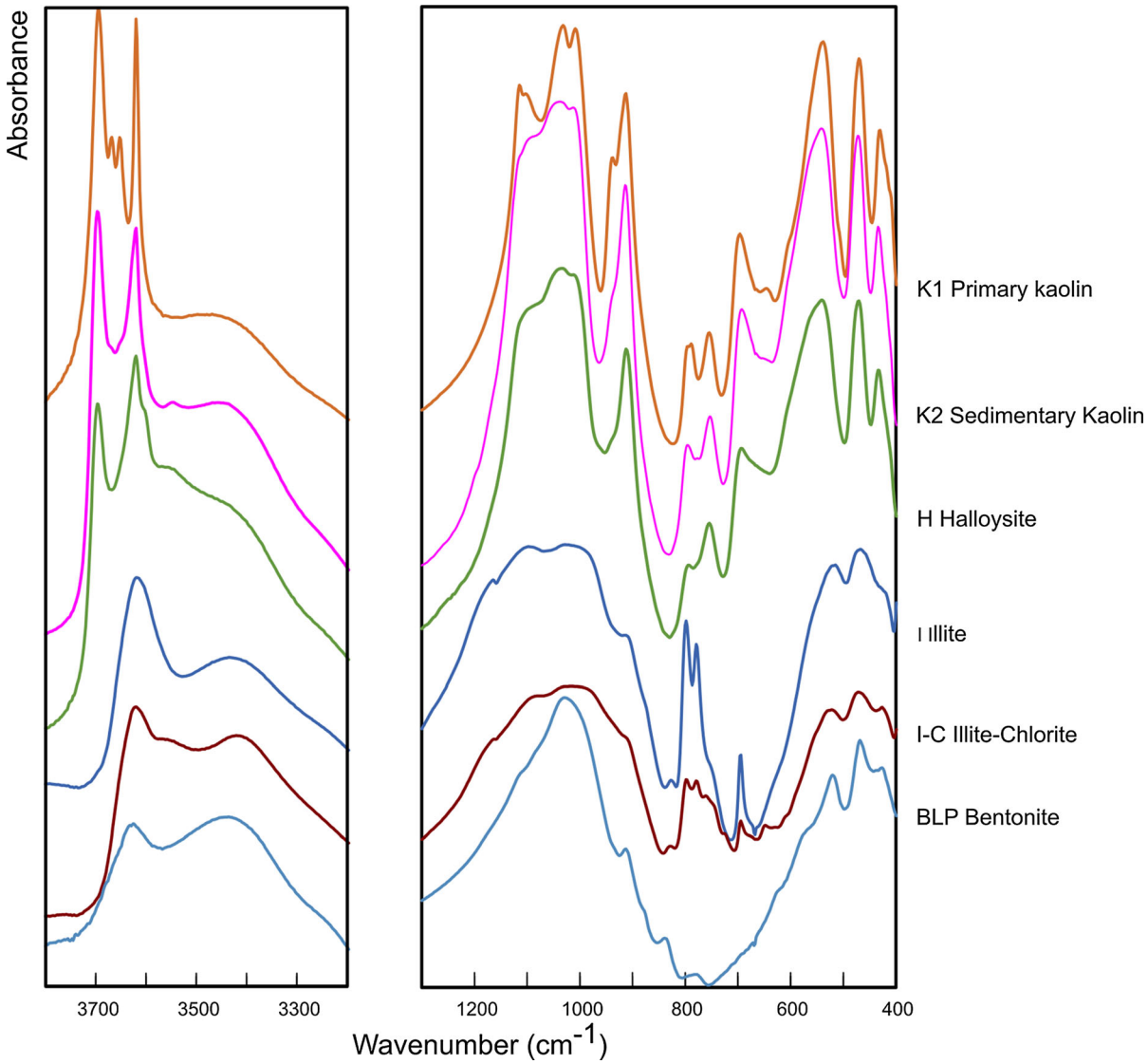

Fig. 8 IR Spectra of raw clays evaluated for use as SCM: **a** and **b** kaolinitic clay [95], **c** halloysite [96]; **d** illitic shale [97]; **e** Illitic-chlorite shale [16], and **f** bentonite [100]

3.4.1.5 Raw clay examples Example FTIR spectra of raw clays evaluated for use as SCM are shown in Fig. 8. For kaolinitic clays (K1 and K2), the characteristic band at 3700 cm^{-1} is isolated from absorption bands of most other clay minerals allowing the identification of very low kaolinite concentrations [85]. The four characteristic bands (3690, 3670, 3650 and 3620 cm-1) are well defined in K1 indicating that K1 contains ordered kaolinite, in K2 the intermediate bands (3670 and 3650) are absent indicating disordered kaolinite [95]. For halloysite clay (H) [96], the bands at 3700 and 3620 cm^{-1} in Fig. 8 are assigned to internal surface OH groups. The weak band at 3570 cm^{-1} present in halloysite may arise from H-bonding between surface OH- groups and interlayer water [92].

For illitic shale [97], the FTIR spectrum (Fig. 8) shows the OH- stretching band at 3624 cm^{-1} accompanied by a strong absorption at 3423 cm^{-1} that is allocated to OH stretching vibrations of water

molecules not released upon heating of the KBr pellet [94]. The Si–O stretching band is present at 1027 cm^{-1}, and a doublet in the 825–750 cm^{-1} range is assigned to the vibration of Si–O–Al moieties [98]. Figure 8 also includes a raw clay (illite-chlorite, I-C) showing a weak inflection at 3680 cm^{-1} and strong bands of OH bending [16]. Bentonite [99] contains montmorillonite showing a OH stretching band at 3623 cm^{-1} [90] and the vibration bands of the different groups of montmorillonites are also present.

Whilst MIR spectroscopy does not offer the same opportunities for quantitative mineralogical analysis as in XRD and STA, its speed and relative simplicity nonetheless offers advantages—particularly for broadly identifying the presence of 1:1 and/or 2:1 clay minerals, based on the number and profile of OH-stretching absorption bands in the 3500–3800 cm^{-1} range, and complementary information about structural ordering.

3.4.2 Remote sensing for clay prospecting

Whilst laboratory-based infrared spectroscopy typically focusses on the near- and mid-infrared spectral range (13,000–1250 cm^{-1}), the visible and near infrared (VNIR) range (25,000–9000 cm^{-1}) offers specific opportunities for remote sensing.

The principle of spectroscopy-based remote sensing is that airborne or satellite-mounted sensors measure the reflectance radiation from the earth's surface for either a small number of wavelength channels (multi-spectral) or a continuum of wavelengths (hyper-spectral). The mineralogy (along with other aspects) of the area can be identified by comparing the measured signals to spectral libraries, and then mapped [101]. Previous studies have used VNIR remote sensing to: map the distribution of different clay minerals in soils [102, 103]; estimate the overall clay content of soils [104], and (in combination with XRD analysis to facilitate supervised classification) map kaolinite deposits by both purity (%kaolinite) and quality (degree of disorder) (Fig. 9) [105].

The key advantage of remote sensing is the potential to produce mineralogical maps of large areas very quickly, with drone-based systems offering an additional advantage of low cost [106]. The main drawbacks and limitations are around measurement (sampling depth, spatial resolution and vegetation cover), as well as the spectral resolution and sensitivity of the instruments themselves. It is also advised not to solely rely on remote measurements, but to support with validation from some terrestrial measurements [107]. More detailed information on the capabilities and limitations of the different instruments and systems available can be found elsewhere [108, 109].

VNIR remote sensing has shown great progress in mapping of soils in recent years (e.g. Global Soils Map project) [110], but has yet to be exploited much for clays prospecting in the cement industry. These techniques could be adapted to play a key role in the triage of analysing deposits in remote and/or poorly documented areas, supporting exploitation of a wider variety of deposits for localised production, especially in developing countries.

4 Case studies

Two exemplary case studies are discussed here to illustrate the mineralogical interpretation and analysis two impure clays, i.e. one quartz-rich kaolinitic clay and one smectitic clay, both originating from the German Westerwald area. Both clays were measured by XRD, TGA and FTIR spectroscopy, the samples were prepared in line with the general guidelines provided in the respective sections.

The XRD measurements are plotted in Fig. 10, measurements were made of a randomly oriented bulk sample of each clay, and of oriented specimens of the clay size fraction (< 2 μm). Air-dried, ethylene glycol (EG) solvated and 550 °C heat treated oriented specimens were prepared and measured to support the mineralogical interpretation. The XRD results show that the kaolinitic clay is mainly composed of the clay minerals kaolinite and illite, together with quartz and traces of other minerals such as feldspars. The identification of kaolinite is confirmed by the absence of its (00l) peaks in the heat treated oriented specimen. The presence of chlorite can be excluded due to the absence of the 7.1 Å peak after heat treatment. The EG treatment did not induce peak shifts, indicating the absence of smectitic or other swellable clay minerals. In contrast, EG induced swelling is clearly observed for the main smectite peaks in the smectitic clay. The EG treatment led to a rational shift of peaks, thus indicating the absence of mixed-layering. The main (060) reflection (not shown) is situated around

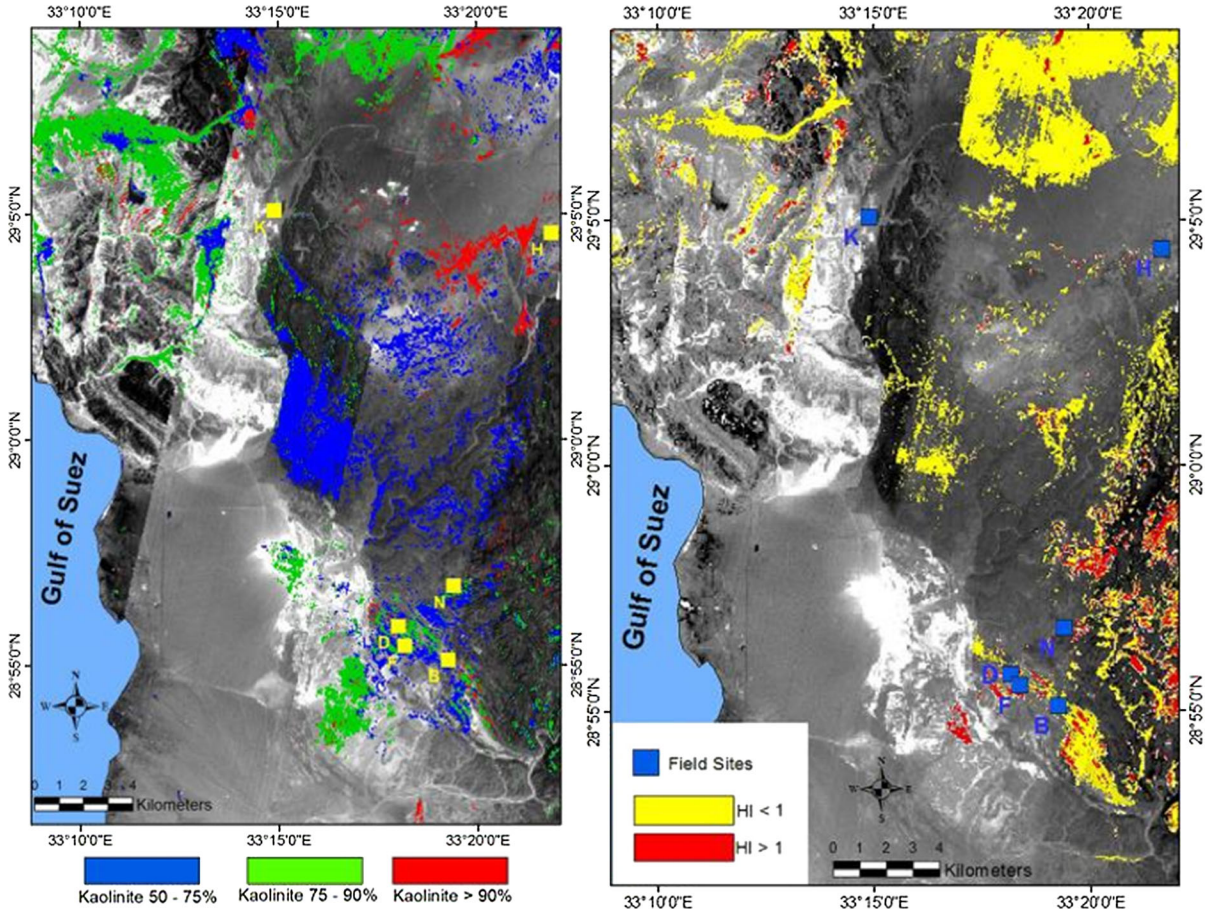

Fig. 9 Hyperspectral maps showing the distribution of **a** kaolin purity and **b** kaolinite Hinckley Index for a kaolin deposit in Egypt. Images reprinted with permission from [105]

1.498 Å, indicating a di-octahedral nature (e.g. Al-rich/montmorillonite) of the main clay minerals. Heat treatment led to a loss of smectite interlayer water and a collapse of the layers. The heat treatment also confirmed the presence of kaolinite and absence of chlorite. In addition, a minor amount of illite can be identified in the smectitic clay.

The TG/DTG and the FTIR data of both clays are presented in Fig. 11. The TG/DTG analysis of the kaolinitic clay shows a major mass loss event from about 500 to 600 °C. This event can be mainly attributed to the dehydroxylation of kaolinite, however the dehydroxylation of illite should also make a minor contribution. The minor mass losses between 70 and 150 °C are associated with loss of weakly-bound interlayer water in illite and physically adsorbed water. The small DTG peak at around 300 °C may be attributed to the dehydroxylation of iron hydroxide (e.g. goethite). The smectitic clay shows two main mass loss events, the low temperature (80–200 °C) mass loss is related to the release of smectite interlayer water and to a minor part of physically adsorbed water, the mass loss in the temperature range of 500 to 600 °C is mainly associated to kaolinite dehydroxylation. Dehydration of the smectite phase (montmorillonite) is visible between 700 and 750 °C.

The FTIR data provide additional information on kaolinite ordering and the dominant cation in the 2:1 clay mineral octahedral sheet. In the kaolinitic clay the P0 index and the absence of the doublet in the OH-stretching vibrations (3694–3620 cm^{-1}) imply a disordered nature of the kaolinite. In the smectitic clay a

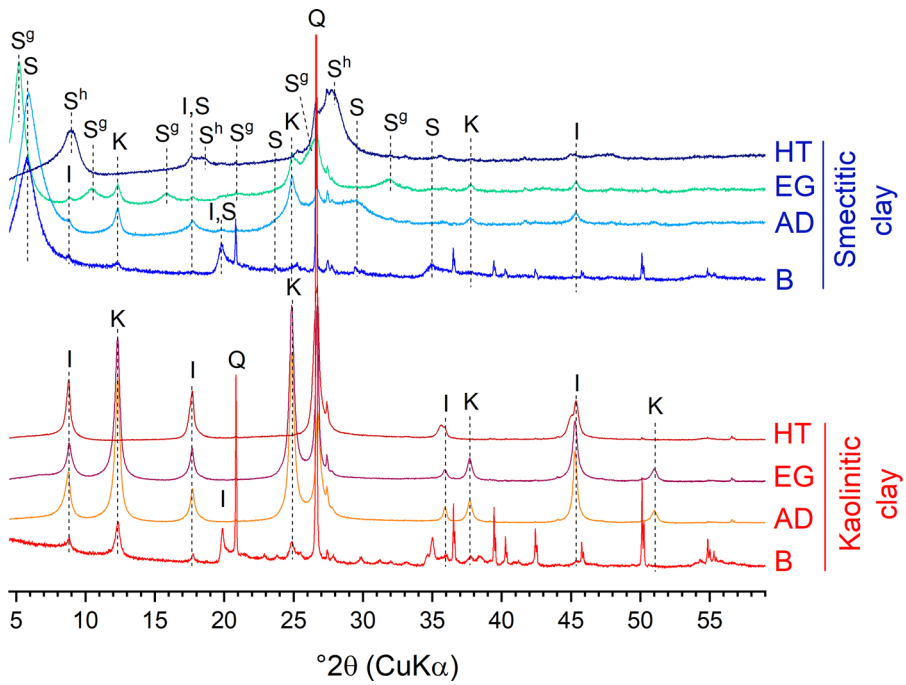

Fig. 10 Interpreted XRD measurements of the case study impure kaolinitic and smectitic clays. XRD measurements were made on randomly oriented bulk samples (B), and on air-dried (AD), ethylene glycol solvated (EG) and 550 °C heat treated (HT) oriented samples of the clay size fraction (< 2 μm). The main reflection peaks are labelled as follows: I stands for illite, K for kaolinite, S for smectite, S^g for glycolated smectite, S^h for heat treated, collapsed smectite, and Q for quartz

similar interpretation is obscured by the presence of the smectite clay. Characteristically the smectite interlayer water shows a broad vibration band around 3400 cm^{-1}. The main vibration band from 970 to 1200 cm-1 is allocated to tetrahedral silicate stretching vibrations. More informative are the position of the octahedral bending vibration bands situated between 850 and 950 cm^{-1}. The Al_2OH moieties in kaolinite show characteristic bands around 910 and 935 cm^{-1}. The former is visible in both clays, the latter only in the kaolinitic clay. The additional vibration band at 875 cm^{-1} in the smectitic clay indicates substitution of Al by Fe^{3+} in the montmorillonite (smectite) octahedral sheet.

Quantitative phase analysis of the bulk samples was made by Rietveld refinement using the software Profex-BGMN [58]. The program allows an implementation of disorder models, e.g. turbostratic disorder in smectites or stacking disorder in kaolinite. In order to retrieve absolute phase contents and the amount of amorphous or unknown phases, the scale factors were normalized to an external standard [46]. Therefore, the mass attenuation coefficient of each sample was calculated, based on the chemical composition.

The quantitative phase analysis is in good agreement with the TGA results. Regarding the kaolinitic clay, a mass loss of 5.4 wt.% occurs between 400 and 1000 °C. The dehydroxylation of kaolinite accounts for 3.8 wt.%, based on its chemical formula and the mass content derived by XRD. This would leave 1.6 wt.% mass loss attributed to illite/muscovite.

Further to the information provided in this article, the interested reader is recommended to seek out the Baseline Studies of the Clay Minerals Society Source Clays[3] [111]. Whilst many advances in terms of techniques have been made since their publication in the early 2000s, they remain a highly useful (and free to access) collection of detailed characterization studies using the techniques described here, carried

[3] Available at Baseline/MSDS studies of source clays—The Clay Minerals Society.

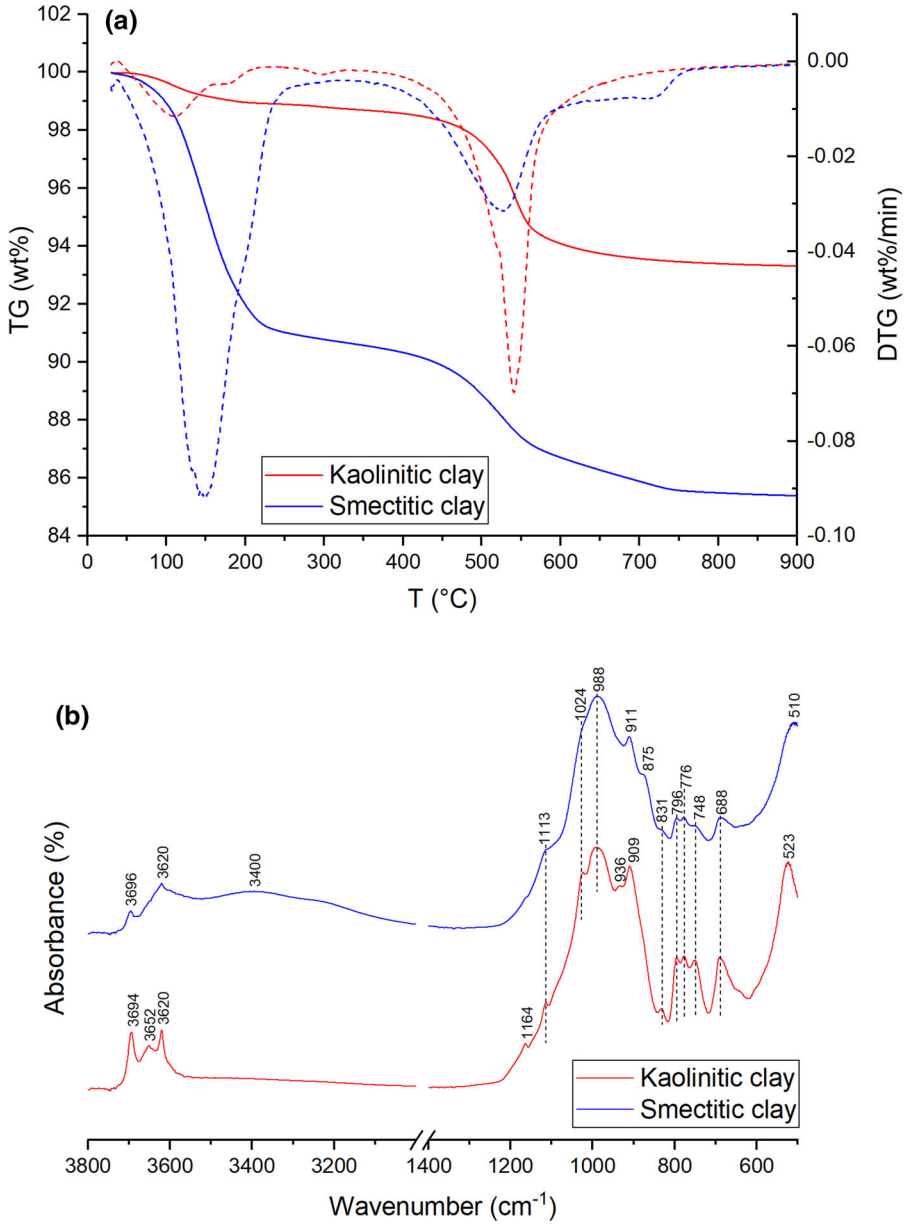

Fig. 11 TG/DTG (**a**) and FTIR (**b**) measurements of the case study impure kaolinitic and smectitic clays. In **a** the TG curves are displayed as solid lines and the DTG curves as dashed lines. In **b** the wavenumbers of the vibration bands are indicated

out on the clay minerals of primary interest to cement scientists.

5 Summary and perspectives

The rapid development of calcined clay blended cements requires accessible and robust techniques to characterise the mineralogical composition of potentially suitable clay resources. Before setting out on clay analysis techniques, this paper stresses the importance of field sampling methodology and sample preparation to obtain representative specimens. If not done properly, any subsequent analysis, no matter how meticulously carried out, risks to be biased and of little use.

Three characterisation techniques were identified to be most relevant: XRD, thermal analysis and IR spectroscopy. They have in common that they are easily accessible and well-established in most cement chemistry laboratories, and have been extensively applied to clay science. Due to the fine-grained and multi-phase nature of clays, and the structural and compositional variability of the clay minerals, mineralogical analysis of clays is often tedious, and practitioners should be aware of potential interferences and limitations. Therefore, for each of the techniques, clay specific sample preparation and data collection routines were described together with guidelines to the interpretation and analysis of the collected data.

XRD is of great practical value in clay mineralogy. Even for highly complex clays and clay minerals, it can provide both highly resolved identification of clay and other minerals and accurate phase quantification. To obtain such information, specific laboratory routines and analytical software are required, using these correctly relies on somewhat advanced understanding and analytical experience.

Thermal analysis can be used more readily and easily, yet does not provide the same level of detail as XRD. Overlap between mass loss events for different clay minerals can be significant. Similarly, structural and chemical variability of individual clay minerals affect the heating profiles considerably. Both phenomena interfere with accurate phase quantification. A notable exception may be kaolinite-group minerals, that show a rather distinct and pronounced dehydroxylation event, enabling a fairly accurate estimation of their total content by thermal analysis.

IR spectroscopy is straightforward to use, but should mainly be seen as a complementary qualitative technique that provides information on structural (dis)order or averaged octahedral layer composition that is more difficult to obtain using XRD and thermal analysis. IR spectroscopy can also be used as identification technique for exploration purposes, such as remote sensing, or made portable for in-situ field measurements. Interpretation is more difficult for complex multi-phase clays.

As clay purity and the type and content of accompanying minerals are important characteristics that define the suitability as SCM resource, mineralogical characterisation is indispensable as source of information. Moreover, to better understand and predict the performance of the broad and heterogeneous group of 2:1 clays, much more detailed research based on a solid and extensive analysis of the clay mineralogy is needed.

Acknowledgements Textual comments and suggestions by Alisa Machner are gratefully acknowledged.

Author contributions Initiation and conceptualisation: RS and AAD; Data provision and processing: MM, RS and EFI; Writing of sections: RS, AAD, TH, EFI, MM, ATM, LV, FZ; Critical revising: FK, RA, TH, MM, ATM, AAD; Coordination, integration and editing: RS and AAD.

Funding Participation of Alastair T. Marsh was funded by EPSRC EP/R001642/1. Participation of T. Hanein was funded by UKRI through the Circular Economy Centre for Mineral-based Construction Materials (EP/V011820/1). The other authors received no support from any organization for the submitted work.

Declarations

Ethical standards The contents of this paper reflect the views of the authors, who are responsible for the validity and accuracy of presented data, and do not necessarily reflect the views of their affiliated organisations.

Competing interests The authors have no competing interests to declare that are relevant to the content of this article.

Appendix 1: XRD search table for clay minerals and commonly associated phases

See Table 3.

Table 3 Search table (modified after Brindley and Brown [7] and Thorez [112])

d	Clay minerals and phyllosilicates	d	Other silicates	*d*	Oxides, hydroxides, carbonates, sulfate, etc
17.0–16.8	Smectite, glycol (10)				
15.5–15	Smectite, Mg Ca (10)				
14.6–14	Vermiculite (10)				
14.3–14.0	Chlorite (3–10), weak if iron-rich				
14.1–13.7	Chlorite, 500–600 °C (10+)				
12.4	Smectite, Na (10)				
12.3–12.0	Sepiolite (10)				
10.5–10.3	Palygorskite (10)				
10.1–10.0	Halloysite—10 Å (7–10)				
10.1–9.9	Muscovite (10) Phlogopite (10)				
	Biotite (10)				
10–9.6	Smectite, collapsed (10)				
	Vermiculite, collapsed (10)				
9.3	Talc (10)	9.10	Mordenite (9)		
9.2–9.1	Pyrophyllite (10)	9.05–8.97	Heulandite-clinoptilolite (6–10)		
8.5	Smectite, glycol (4)	8.5–8.2	Amphiboles (10)		
		7.94–7.89	Heulandite clinoptilolite (2–6)	7.6	Gypsum (10)
7.35–7.25	Serpentine (10)				
7.2–7.1	Chlorite (6–10) Al-serpentine (10)				
7.15	Kaolinite (10)				
		6.61	Mordenite (9)	6.26	Lepidocrocite (10)
				6.11	Boehmite (10)
				6.01	Bassanite (10)
				5.97–5.93	Jarosites (2–5)
		5.61	Analcime (6)	5.49	Mirabilite (10)
		5.39	Mullite (5)		
5.05–4.95	Muscovite (4–5)			5.10–5.06	Jarosites (7–10)
		4.85	Analcime (2)	4.85	Gibbsite (10)
4.8	Vermiculite (2)			4.77	Brucite (9)
4.78–4.68	Chlorites (4–8)			4.77	Mirabilite (5)
4.66–4.56	Smectite (5)	4.68–4.64	Heulandite-clinoptilolite (2–7)	4.73–4.66	Spinels (2)
4.66	Talc (3)				
4.60–4.57	Serpentines (3–6)				
4.60	Vermiculite (5)				
4.55	Talc (3)				
4.50–4.47	Palygorskite (5)	4.43	Zircon (5)	4.37	Gibbsite (5)
	Sepiolite (3)				
4.49–4.45	Mica, dioctahedral (5–9); Smectite, dioctahedral (5)				
4.48–4.44	Kaolinite (4–8)				
4.44	Halloysite (9)	4.33–4.30	Opal-CT (7)	4.28–4.27	Gypsum (5)
4.36	Kaolinite (7) Dickite (7)	4.26	Quartz, low (3)	4.26	Vaterite (7)

Table 3 continued

d	Clay minerals and phyllosilicates	d	Other silicates	*d*	Oxides, hydroxides, carbonates, sulfate, etc
4.31	Sepiolite (4)	4.23–4.21	K-feldspars (6)		
		4.21–4.04	K-Na feldspars (6–7)	4.18–4.15	Goethite (10)
		4.11–4.09	Opal-CT (10)		
		4.04–4.02	Na and Ca feldspars (5–8)		
		4.00	Mordenite (9)		
		3.97–3.95	Heulandite-clinoptilolite	3.99	Diaspore (10)
3.89	Muscovite $2M_1$ (4)			3.90	Baryte (6)
		3.83–3.70	Feldspars (7)	3.85	Sulphur (10)
3.66	Muscovite 1 *M (6)*			3.73	Ilmenite (5)
3.66–3.61	Serpentine (3–6)			3.67	Hematite (3)
3.60–3.50	Chlorite (7–10) Al-serpentine (4)	3.67-3.62	Na and Ca-feldspars (2–4)	3.65	Jarosites (4)
3.60–3.58	Vermiculite (3)				
3.59–3.58	Kaolinite (7)	3.48	Mordenite (10)	3.52	Anatase (10)
		3.43	Analcime (10)	3.48	Corundum (8)
3.40	Smectite, glycol (5); Halloysite—10 Å (5)	3.42	Sillimanite (10)	3.44	Sulphur (4), Baryte (10)
		3.39	Mullite (10) Mordenite (9)	3.40	Aragonite (10)
3.37–3.34	Sepiolite (4)	3.34	Quartz, low (10)	3.36	Graphite (10)
		3.31–3.29	K-feldspars (10)	3.32	Baryte (10)
		3.30	Zircon (10)	3.30	Vaterite (10)
		3.26–3.25	Ca-feldspars (3–5)	3.27	Aragonite (5)
		3.26–3.23	K-feldspars, 2 lines (4–10)	3.25	Rutile (10)
3.24	Palygorskite (5–10)	3.25–3.15	Pyroxenes (4–10)	3.21	Sulphur (6)
3.21	Muscovite $2M_1$ (4)	3.21–3.15	Na and Ca feldspars, 2 or 3 lines including strongest (2–10)	3.15	Sylvite (10) Fluorite (9)
		3.13–3.12	Ca-feldspars, albite (2–4)	3.13–3.11	Jarosites (7–9)
3.12	Talc (6)	3.13–3.05	Amphiboles	3.12	Pyrite (4)
3.10	Smectite, Na (5)			3.10	Baryte (10)
				3.09–3.06	Jarosites (7–10)
3.07	Muscovite 1 *M* (5) Pyrophyllite (10)	3.04–2.89	Plagioclase feldspars, 2, 3, or 4 Lines (1–3)	3.08–3.06	Gypsum (6)
3.0	Muscovite, $2M_1$ (4)	3.02–2.94	Pyroxenes (4–10)	3.04	Calcite (10) Vaterite (10)
3.0	Smectite, Mg, Ca (4–7)	2.99	K-feldspars, monoclinic (5)	3.00	Bassanite (10)
		2.99–2.96	Heulandite-clinoptilolite (5–8)	2.97–2.95	Magnetite-maghemite (3)
		2.93	Analcime (5)	2.89	Dolomite (10)
2.88	Vermiculite (4)	2.91–2.87	Pyroxenes (4–10)	2.90–2.86	Spinels (4)
2.87	Muscovite $2M_1$ (4)			2.82	Halite (10)
2.86–2.82	Vermiculite (4)	2.81–2.77	Olivine (6–10)	2.81–2.77	Apatites two lines (6–10)
				2.80	Bassanite (5)
				2.79	Siderite (10)
		2.75–2.69	Amphibole (10)	2.73	Vaterite (10)
				2.72–2.69	Apatites (6–10)

Table 3 continued

d	Clay minerals and phyllosilicates	d	Other silicates	*d*	Oxides, hydroxides, carbonates, sulfate, etc
				2.71	Pyrite (10)
2.66–2.64	Biotite (8) Serpentines (5)	2.69	Analcime (2) Mullite (4)	2.69	Hematite (10)
2.60–2.55	Smectite, Muscovite (4–10) Chlorite (1–6)	2.60–2.53	Pyroxene (5–10)	2.55	Corundum (9)
2.56	Kaolinite (6)			2.53–2.51	Magnetite-maghemite (10)
		2.49–2.46	Olivine (7–10)	2.51	Hematite (7)
2.46–2.43	Chlorite (2–8)			2.49	Rutile (5)
				2.47–2.44	Spinel (10)
2.39	Kaolinite (8)			2.45–2.43	Goethite (6)
2.375	Serpentines (8)			2.42	Pyrite (7)
				2.37	Brucite (10)
		2.30–2.25	Olivine (2–4)	2.35	Boehmite (6)
		2.20	Mullite (6) Sillimanite (6)	2.21	Pyrite (5) Anhydrite (2)
2.16–2.13	Serpentines (2–8)			2.12	Baryte (8)
		2.07	Zircon (2)	2.07	Pyrrhotite (10)
2.05–1.99	Chlorites (2–6)			2.06	Vaterite (10)
2.01–1.99	Muscovite (3–5)			2.03	Graphite (5)
1.989	Kaolinite (6)			1.994	Halite (5)
				1.977	Aragonite (6)
				1.931	Fluorite (10)
1.870	Talc (4)	1.817	Quartz, low (2)	1.838	Hematite (3)
		1.77–1.75	Olivine (4)	1.726	Ilmenite (6)
1.72–1.68	Smectite (1–5)	1.712	Zircon (4)	1.692	Hematite (5)
				1.687	Rutile (6)
1.662	Kaolinite (7)			1.647	Fluorite (4)
				1.633	Pyrite (10)
1.619	Kaolinite (6)			1.617–1.614	Magnetite-maghemite (3)
1.58–1.52	Chlorite (2–7)			1.601	Corundum (8)
				1.576–1.555	Spinels (4)
				1.573	Brucite (4)
1.54–1.49	Smectite (2–6)	1.541	Quartz (2)		
1.537	Vermiculite (5)				
1.527	Talc (5)	1.525	Mullite (5)		
		1.519	Sillimanite (3)		
1.503–1.499	Muscovite (4)				
1.489	Kaolinite (8)			1.485–1.474	Magnetite-maghemite (4)
1.484	Halloysite (5)			1.484	Hematite (2)
				1.469	Ilmenite (3)
1.452	Kaolinite (4)			1.452	Hematite (3)
				1.448–1.429	Spinels (6)

Appendix 2: Main IR vibration bands of common clay minerals (after [113])

Clay mineral	Formula	Wavenumber, cm^{-1} *
Kaolinite	$Al_2Si_2O_5(OH)_4$	3693s, 3655sh, 3620, 1115s, 1090s, 1032s, 1006s, 939, 914s, 792, 753, 696, 642, 600sh, 536s, 470s, 429
Dickite	$Al_2Si_2O_5(OH)_4$	3708, 3655, 3625, 1118s, 1080, 1033s, 1004s, 965sh, 937, 914, 795, 755w, 697, 600sh, 534s, 467s, 425
Nacrite	$Al_2Si_2O_5(OH)_4$	3710, 3660, 3640, 1120s, 1100s, 1036s, 1003s, 930sh, 913, 799w, 754w, 696, 600sh, 535s, 468s, 424
Halloysite-10 Å	$Al_2Si_2O_5(OH)_4{\cdot}2H_2O$	3615, 3525w, 3395, 1630w, 1075s, 1037s, 1023s, 827w, 788, 743w, 676, 617w, 590sh, 490sh, 468s
Halloysite	$Al_2Si_2O_5(OH)_4{\cdot}nH_2O$	697w, 3620, 3380, 1630w, 1090sh, 1028s, 1020sh, 913, 790sh, 750w, 671, 533, 495sh, 471s, 435sh
Pyrophyllite	$Al_2Si_4O_{10}(OH)_2$	3678, 1120s, 1068s, 1050s, 950s, 854, 836, 814, 737w, 620, 578, 539s, 519, 481s, 458, 414
Saponite	$(Ca_{0.5},Na)_{0.3}(Mg,Fe^{2+})_3[(Si,Al)_4O_{10}](OH)_2{\cdot}4H_2O$	3635, 3430sh, (3330), 1650w 1002s, 770w, 730w, 665, 459s
Hectorite	$Na_{0.3}(Mg,Li)_3(Si_4O_{10})(F,OH)_2$	3682w, 3640w, 3450w, 1625w, 1065sh, 1010s, 900sh, 701, 687, 677, 656, 520sh, 464s
Stevensite	$Ca_xMg_3[(Si,Al)_4O_{10}](OH)_2{\cdot}\ nH_2O$ ($\times$ *0.15, n 2*)	3450, 1638, 1023s, 669, 525sh, 470s, 453s
Montmorillonite	$(Na,Ca)_{0.3}(Al,Mg)_2(Si_4O_{10})(OH)_2{\cdot}nH_2O$	3620, 3430w, 1620w, 989, 923s, 912s, 800w, 701s, 607, 540s, 486s
Beidellite	$(Na,Ca_{0.5},K)xAl_2[(Si,Al)_4O_{10}](OH)_2{\cdot}nH_2O$ ($\times$ *0.3*)	3590, 3415, 1640w, 1110sh, 1033s, 1010sh, 935sh, 912, 697w, 534s, 473s, 423s
Nontronite	$(Na,Ca)_x(Fe^{3+},Al,Mg)_2[(Si,Al)_4O_{10}](OH)_2{\cdot}nH_2O$ ($\times$ *0.3, n 4*)	557, 3390, 3240sh, 1650sh, 1632, 1100sh, 1021s, 940sh, 847, 817, 745w, 675, 585, 492s, 450sh, 430s, 380s
Vermiculite	$(Mg,Fe,Al)_3[(Si,Al)_4O_{10}](OH)_2{\cdot}4H_2O$	3550sh, 3375, 3250sh, 1657, 1070sh, 991s, 819w, 730sh, 710sh, 680sh, 657, 510sh, 450s, 420sh
Illite	$K_{0.65}Al_2(Si_{3.35}Al_{0.65}O_{10})(OH)_2$	3620, 3420, 1665w, 1635w, 1080sh, 1023s, 1000sh, 915, 825sh, 754w, 700w, 605sh, 525s, 471s, 425sh
Glauconite	$K_{1-x}(Fe^{3+},Mg,Fe^{2+},Al)_2[Si_3(Si,Al)O_{10}](OH)_2$	3645sh, 3600sh, 3560, 3540sh, 3365, 3240sh, 1630w, 1120sh, 1029s, 995sh, 877, 819w, 677w, 489s, 460s, 431sh
Phlogopite	$KMg_3(Si_4AlO_{10})(OH)_2$	3695, 3675, 3375, 1740w, 1660sh, 1640, 995s, 818, 760sh, 726, 689, 650, 606, 520sh, 490sh, 459s, 430sh
Muscovite	$KAl_2(Si_3AlO_{10})(OH)_2$	3570, 3385, 1610w, 1070sh, 1023s, 999s, 906, 826, 744w, 660w, 600sh, 520s, 469s, 417
Clinochlore	$(Mg,Al)_6(Si,Al)\ _4O_{10}\ (OH)_8$	3670, 3615sh, 3580, 3440, 1085sh, 1061, 996s, 961s, 815, 648, 526, 490sh, 455s, 437s, 415sh
Clinochlore	$(Mg,Al)_6(Si,Al)_4O_{10}\ (OH)_8$	3630sh, 3570, 3440sh, 1635w, 1045sh, 993s, 962s, 812w, 795w, 710sh, 650, 610sh, 446s
Chamosite	$(Fe,Al,Mg)_6(Si,Al)\ _4O_{10}\ (OH)$	3540, 3360, 3220sh, 981s, 746, 659, 610, 446s, 420sh
Sepiolite	$Mg_4(Si_6O_{15})(OH)_2{\cdot}6H_2O$	3625sh, 3577, 3395, 3230sh, 1654, 1625sh, 1205, 1065sh, 1019s, 980sh, 782w, 728w, 686, 643, 530sh, 495sh, 466s, 440sh, 420sh
Palygorskite	$(Mg,Al)_{2+x}(Si_4O_{10})(OH){\cdot}4H_2O$	3615, 3580, 3415, 3280sh, 1660, 1197, 1119, 1083, 1040s, 986s, 909w, 870w, 680sh, 643w, 570, 540sh, 511, 484s, 438

**s* strong, *w* weak, *sh* shoulder

References

1. Juenger MC, Snellings R, Bernal SA (2019) Supplementary cementitious materials: new sources, characterization, and performance insights. Cem Concr Res 122:257–273
2. Scrivener K et al (2018) Calcined clay limestone cements (LC3). Cem Concr Res 114:49–56
3. Scrivener KL, John VM, Gartner EM (2016) Eco-efficient cements: potential, economically viable solutions for a low-CO_2, cement-based materials industry. In: UNEP Report. United Nations Environment Programme, Paris, pp 50
4. Maier M, Beuntner N, Thienel K-C (2021) Mineralogical characterization and reactivity test of common clays suitable as supplementary cementitious material. Appl Clay Sci 202:105990
5. Hollanders S et al (2016) Pozzolanic reactivity of pure calcined clays. Appl Clay Sci 132:552–560
6. Skibsted J, Snellings R (2019) Reactivity of supplementary cementitious materials (SCMs) in cement blends. Cem Concr Res 124:105799
7. Brindley G, Brown G (1980) Quantitative X-ray mineral analysis of clays. In: Crystal structures of clay minerals and their X-ray identification, vol 5. Mineralogical Society, London, pp 411–438
8. Moore DM, Reynolds RCJ (1997) X-ray diffraction and the identification and analysis of clay minerals, 2nd edn. Oxford University Press (OUP), Oxford
9. Raven MD, Self PG (2017) Outcomes of 12 years of the Reynolds Cup quantitative mineral analysis round robin. Clays Clay Miner 65(2):122–134
10. Omotoso O et al (2006) Some successful approaches to quantitative mineral analysis as revealed by the 3rd Reynolds Cup contest. Clays Clay Miner 54(6):748–760
11. Środoń J (2006) Identification and quantitative analysis of clay minerals. Dev Clay Sci 1:765–787
12. Avet F, Scrivener K (2018) Investigation of the calcined kaolinite content on the hydration of Limestone Calcined Clay Cement (LC3). Cem Concr Res 107:124–135
13. Alujas A et al (2015) Pozzolanic reactivity of low grade kaolinitic clays: Influence of calcination temperature and impact of calcination products on OPC hydration. Appl Clay Sci 108:94–101
14. Snellings R et al (2016) Properties and pozzolanic reactivity of flash calcined dredging sediments. Appl Clay Sci 129:35–39
15. Danner T, Norden G, Justnes H (2018) Characterisation of calcined raw clays suitable as supplementary cementitious materials. Appl Clay Sci 162:391–402
16. Irassar EF et al (2019) Calcined illite-chlorite shale as supplementary cementing material: thermal treatment, grinding, color and pozzolanic activity. Appl Clay Sci 179:105143
17. Konta J, Kühnel R (1997) Integrated exploration of clay deposits: some changes of strategy. Appl Clay Sci 11(5–6):273–283
18. Andresen A (1981) Exploration, sampling and in-situ testing of soft clay. In Brand EW, Brenner RP (Ed) Soft Clay Engineering. Dev Geotech Eng 20:239–308
19. Potts PJ, Robinson P (2003) Sample preparation of geological samples, soils and sediments. In Mester Z, Sturgeon R (Ed) Sample Preparation for Trace Element Analysis, Elsevier, Amsterdam. Compr Analyt Chem 41:723–763
20. Potts PJ, West M (2008) Portable X-ray fluorescence spectrometry: capabilities for in situ analysis. Royal Society of Chemistry, London. Cambridge, pp 141–173
21. Rousseau R (2001) Concept of the influence coefficient. Rigaku J 18(1):8–14
22. Ichikawa S, Nakamura T (2016) Approaches to solid sample preparation based on analytical depth for reliable X-ray fluorescence analysis. X-Ray Spectrom 45(6):302–307
23. Hou X, He Y, Jones BT (2004) Recent advances in portable X-ray fluorescence spectrometry. Appl Spectrosc Rev 39(1):1–25
24. Weindorf DC, Bakr N, Zhu Y (2014) Advances in portable X-ray fluorescence (PXRF) for environmental, pedological, and agronomic applications. Adv Agron 128:1–45
25. Horta A et al (2015) Potential of integrated field spectroscopy and spatial analysis for enhanced assessment of soil contamination: a prospective review. Geoderma 241:180–209
26. Liangquan G (2008) Geochemical prospecting. In: Potts PJ, West M (Eds) Portable X-ray fluorescence spectrometry. Royal Society of Chemistry, Cambridge, pp 141–173
27. Stockmann U et al (2016) Utilizing portable X-ray fluorescence spectrometry for in-field investigation of pedogenesis. CATENA 139:220–231
28. Silva SHG et al (2018) Soil weathering analysis using a portable X-ray fluorescence (PXRF) spectrometer in an Inceptisol from the Brazilian Cerrado. Appl Clay Sci 162:27–37
29. Olesik JW (1996) Fundamental research in ICP-OES and ICPMS. Anal Chem 68(15):469A-474A
30. Carter JA et al (2018) Traditional calibration methods in atomic spectrometry and new calibration strategies for inductively coupled plasma mass spectrometry. Front Chem 6:504
31. Batista AH, Gilkes RJ, Rate AW (2016) Relationship between heavy metals and minerals extracted from soil clay by standard and novel acid extraction procedures. Environ Monit Assess 188(12):1–18
32. Janotková I et al (2013) Comparison of inductively coupled plasma optical emission spectrometry, energy dispersive X-ray fluorescence spectrometry and laser ablation inductively coupled plasma mass spectrometry in the elemental analysis of agricultural soils. J Anal At Spectrom 28(12):1940–1948
33. Khalifa AZ et al (2019) Comparing the reactivity of different natural clays under thermal and alkali activation. RILEM Tech Lett 4:74–80
34. Bergaya F, Theng BKG, Lagaly G (2006) Chapter 12 critical assessment of some analytical techniques. Dev Clay Sci 1:753–754
35. Jackson ML (2005) Soil chemical analysis: advanced course. UW-Madison Libraries Parallel Press, Madison

36. Poppe L et al (2001) A laboratory manual for X-ray powder diffraction. US Geol Surv Open-File Rep 1(041):1–88
37. Środoń J (2013) Chapter 2.2-identification and quantitative analysis of clay minerals. Dev Clay Sci 5:25–49
38. Kleeberg R, Monecke T, Hillier S (2008) Preferred orientation of mineral grains in sample mounts for quantitative XRD measurements: How random are powder samples? Clays Clay Miner 56(4):404–415
39. Bish DL, Reynolds R (2018) 4. Sample preparation for X-ray diffraction. In: Bish DL, Post JE (eds) Modern powder diffraction. De Gruyter, Berlin, pp 73–100
40. Steudel A, Emmerich K (2013) Strategies for the successful preparation of homoionic smectites. Appl Clay Sci 75:13–21
41. Méring J (1949) L'interférence des rayons X dans les systèmes à stratification désordonée. Acta Crystallogr A 2(6):371–377
42. Ufer K, Kleeberg R, Monecke T (2015) Quantification of stacking disordered Si–Al layer silicates by the Rietveld method: application to exploration for high-sulphidation epithermal gold deposits. Powder Diffr 30(S1):S111
43. Madsen IC, Scarlett NVY, Webster NAS (2012) Quantitative phase analysis. In Kolb U, Shankland K, Meshi L, Avilov A, David W (Eds) Uniting Crystallography and Powder Diffraction. NATO Science for PEace and Security Series B: Physics and Biophysics. Springer, Dordrecht pp 207–218
44. Zhou X et al (2018) XRD-based quantitative analysis of clay minerals using reference intensity ratios, mineral intensity factors, Rietveld, and full pattern summation methods: a critical review. Solid Earth Sci 3(1):16–29
45. Hillier S (2000) Accurate quantitative analysis of clay and other minerals in sandstones by XRD: comparison of a Rietveld and a reference intensity ratio (RIR) method and the importance of sample preparation. Clay Miner 35(1):291–302
46. O'Connor BH, Raven MD (1988) Application of the Rietveld refinement procedure in assaying powdered mixtures. Powder Diffr 3(1):2–6
47. Środoń J (2006) Chapter 12.2 identification and quantitative analysis of clay minerals. Dev Clay Sci 1:765–787
48. Bish DL, Howard S (1988) Quantitative phase analysis using the Rietveld method. J Appl Crystallogr 21(2):86–91
49. Butler BM, Hillier S (2021) Automated full-pattern summation of X-ray powder diffraction data for high-throughput quantification of clay-bearing mixtures. Clays Clay Miner 69:38–51
50. Chipera SJ, Bish DL (2002) FULLPAT: a full-pattern quantitative analysis program for X-ray powder diffraction using measured and calculated patterns. J Appl Crystallogr 35(6):744–749
51. Mystkowski K, Srodon J, McCarty D (2002) Application of evolutionary programming to automatic XRD quantitative analysis of clay-bearing rocks. In: The Clay Minerals Society 39th annual meeting, Boulder, Colorado, Abstracts with Programs
52. Eberl D (2003) User guide to RockJock-A program for determining quantitative mineralogy from X-ray diffraction data. US Geological Survey
53. Butler B, Hillier S (2020) powdR: full pattern summation of X-ray powder diffraction data. In: R package version
54. Butler BM, Hillier S (2021) powdR: an R package for quantitative mineralogy using full pattern summation of X-ray powder diffraction data. Comput Geosci 147:104662
55. Rietveld HM (1969) A profile refinement method for nuclear and magnetic structures. J Appl Crystallogr 2(2):65–71
56. Ufer K, Raven MD (2017) Application of the Rietveld method in the Reynolds cup contest. Clays Clay Miner 65(4):286–297
57. Bergmann J, Kleeberg R (1998) Rietveld analysis of disordered layer silicates. In: Delhez R, Mittemeijer EJ (eds) Materials Science Forum 278-281:300–305
58. Doebelin N, Kleeberg R (2015) Profex: a graphical user interface for the Rietveld refinement program BGMN. J Appl Crystallogr 48(5):1573–1580
59. Coelho AA, Evans JS, Lewis JW (2016) Averaging the intensity of many-layered structures for accurate stacking-fault analysis using Rietveld refinement. J Appl Crystallogr 49(5):1740–1749
60. Coelho AA (2018) TOPAS and TOPAS-Academic: an optimization program integrating computer algebra and crystallographic objects written in C++. J Appl Crystallogr 51(1):210–218
61. Scarlett NVY, Madsen IC (2006) Quantification of phases with partial or no known crystal structures. Powder Diffr 21(04):278–284
62. Aranda MA, De la Torre AG, León-Reina L (2012) Rietveld quantitative phase analysis of OPC clinkers, cements and hydration products. Rev Miner Geochem 74(1):169–209
63. Todor DN (1976) Thermal analysis of minerals. Abacus Press
64. Karathanasis A, Harris W (1994) Quantitative thermal analysis of soil materials. In: Chair JEA, Stucki JW (eds) Quantitative methods in soil mineralogy, Soil Science Society of America, Madison, pp 360–411
65. Le Chatelier H (1887) De l'action de la chaleur sur les argiles. Bulletin de Minéralogie 10(5):204–211
66. Giese R (1990) Differential scanning calorimetry of clay minerals and their intercalates. In: Thermal analysis in clay science. Clay Minerals Society, pp 10–48
67. Rouquerol F, Rouquerol J, Llewellyn P (2013) Thermal analysis. In: Bergaya F, Lagaly G (eds) Thermal analysis in clay science. Elsevier, Amsterdam, pp 361–379
68. Földvári M (2011) Handbook of thermogravimetric system of minerals and its use in geological practice, vol 213. Geological Institute of Hungary Budapest, Budapest
69. Bish DL, Duffy CJ, Giese RF (1990) Thermal analysis in clay science. CMS workshop lectures, vol 3. The Clay Minerals Society, Boulder, p 192
70. Karathanasis A, Hajek B (1982) Revised methods for rapid quantitative determination of minerals in soil clays. Soil Sci Soc Am J 46(2):419–425
71. Vaculikova L et al (2011) Characterization and differentiation of kaolinites from selected Czech deposits using infrared spectroscopy and differential thermal analysis. Acta Geodyn Geomater 8(1):59–67

72. Smykatz-Kloss W (1974) The determination of the degree of (dis-) order of kaolinites by means of differential thermal analysis. Chem Erde 33:358–364
73. Ptáček P et al (2013) The influence of structure order on the kinetics of dehydroxylation of kaolinite. J Eur Ceram Soc 33(13–14):2793–2799
74. Lorentz B et al (2018) Characterization of Florida kaolin clays using multiple-technique approach. Appl Clay Sci 161:326–333
75. Plante AF, Fernández JM, Leifeld J (2009) Application of thermal analysis techniques in soil science. Geoderma 153(1–2):1–10
76. Fernandez R, Martirena F, Scrivener KL (2011) The origin of the pozzolanic activity of calcined clay minerals: a comparison between kaolinite, illite and montmorillonite. Cem Concr Res 41(1):113–122
77. Marsh A et al (2019) Influence of clay minerals and associated minerals in alkali activation of soils. Constr Build Mater 229:116816
78. Mackenzie R, Caillere S (1975) The thermal characteristics of soil minerals and the use of these characteristics in the qualitative and quantitative determination of clay minerals in soils. In: Gieseking JE (ed) Soil components. Springer, Berlin, pp 529–571
79. Hayakawa T et al (2016) Modified method for bentonite purification and characterization; a case study using bentonite from Tsunagi Mine, Niigata, Japan. Clays Clay Miner 64(3):275–282
80. Alujas A et al (2015) Pozzolanic reactivity of low grade kaolinitic clays: influence of mineralogical composition. In: Scrivener K, Favier A (eds) Calcined clays for sustainable concrete. Springer, Berlin, pp 339–345
81. Avet F, Scrivener K (2020) Simple and reliable quantification of kaolinite in clay using an oven and a balance. Calcined clays for sustainable concrete, RILEM Book series. Springer, Dordrecht, vol 15, pp 147–156
82. Bernal SA et al (2017) Characterization of supplementary cementitious materials by thermal analysis. Mater Struct 50(1):1–13
83. Chryssikos G (2017) Modern Infrared and Raman instrumentation and sampling methods. Dev Clay Sci 8:34–63
84. Gates W et al (2017) Infrared and Raman spectroscopies of clay minerals. Elsevier, Amsterdam
85. Madejova J, Komadel P (2001) Baseline studies of the clay minerals society source clays: infrared methods. Clays Clay Miner 49(5):410–432
86. Madejová J, Gates W, Petit S (2017) IR spectra of clay minerals. Dev Clay Sci 8:107–149
87. Hutengs C et al (2018) Comparison of portable and benchtop spectrometers for mid-infrared diffuse reflectance measurements of soils. Sensors 18(4):993
88. Balan E et al (2001) First-principles modeling of the infrared spectrum of kaolinite. Am Miner 86(11–12):1321–1330
89. Balan E et al (2005) First-principles study of OH-stretching modes in kaolinite, dickite, and nacrite. Am Miner 90(1):50–60
90. Madejová J (2003) FTIR techniques in clay mineral studies. Vib Spectrosc 31(1):1–10
91. Bich C, Ambroise J, Péra J (2009) Influence of degree of dehydroxylation on the pozzolanic activity of metakaolin. Appl Clay Sci 44(3–4):194–200
92. Russell J, Fraser A (1994) Infrared methods. In: Wilson MJ (ed) Clay mineralogy: spectroscopic and chemical determinative methods. Springer, Berlin, pp 11–67
93. Hillier S et al (2016) Correlations among the mineralogical and physical properties of halloysite nanotubes (HNTs). Clay Miner 51(3):325–350
94. Farmer VC (1974) Infrared spectra of minerals. Mineralogical Society, London
95. Tironi A et al (2014) Potential use of Argentine kaolinitic clays as pozzolanic material. Appl Clay Sci 101:468–476
96. Tironi A et al (2017) Pozzolanic activity of calcined halloysite-rich kaolinitic clays. Appl Clay Sci 147:11–18
97. Irassar EF et al (2019) Thermal treatment and pozzolanic activity of calcined clay and shale. ACI Mater J 116(4):133–143
98. Vaculikova L, Plevova E (2005) Identification of clay minerals and micas in sedimentary rocks. Acta Geodynamica et geomaterialia 2(2):163
99. Tironi A et al (2012) Kaolinitic calcined clays: factors affecting its performance as pozzolans. Constr Build Mater 28(1):276–281
100. Tironi A et al (2012) Thermal activation of bentonites for their use as pozzolan. Revista de la Construccion 11(1):44–53
101. Mulder V et al (2011) The use of remote sensing in soil and terrain mapping—a review. Geoderma 162(1–2):1–19
102. Chabrillat S et al (2002) Use of hyperspectral images in the identification and mapping of expansive clay soils and the role of spatial resolution. Remote Sens Environ 82(2–3):431–445
103. Mulder V et al (2013) Characterizing regional soil mineral composition using spectroscopy and geostatistics. Remote Sens Environ 139:415–429
104. Gasmi A et al (2019) Surface soil clay content mapping at large scales using multispectral (VNIR–SWIR) ASTER data. Int J Remote Sens 40(4):1506–1533
105. Awad ME et al (2018) Hyperspectral remote sensing for mapping and detection of Egyptian kaolin quality. Appl Clay Sci 160:249–262
106. Zhong Y et al (2018) Mini-UAV-borne hyperspectral remote sensing: From observation and processing to applications. IEEE Geosci Remote Sens Mag 6(4):46–62
107. Kirsch M et al (2018) Integration of terrestrial and drone-borne hyperspectral and photogrammetric sensing methods for exploration mapping and mining monitoring. Remote Sens 10(9):1366
108. Fang Q et al (2018) Visible and near-infrared reflectance spectroscopy for investigating soil mineralogy: a review. J Spectrosc 2018:1–14
109. Van der Meer FD et al (2012) Multi-and hyperspectral geologic remote sensing: a review. Int J Appl Earth Obs Geoinf 14(1):112–128
110. Arrouays D et al (2017) McBratney AB, McKenzie NJ, Mendonca-Santos MdL, Minasny B, Montanarella L, Odeh IOA, Sanchez PA, Thompson JA et Zhang G-L, 2014-GlobalSoilMap: toward a fine-resolution global grid of soil properties. Adv Agron 125:93–134

111. Costanzo PM (2001) Baseline studies of the clay minerals society source clays: Introduction. Clays Clay Miner 49(5):372–373
112. Thorez J (1975) Phyllosilicates and clay minerals: a laboratory handbook for their X-ray diffraction analysis
113. Chukanov NV (2013) Infrared spectra of mineral species: extended library. Springer, Berlin